Draft version February 1, 2022
Typeset using LaTeX **twocolumn** style in AASTeX62

IN SEARCH OF THE SHORT GAMMA-RAY BURST OPTICAL COUNTERPART WITH THE ZWICKY TRANSIENT FACILITY

Tomás Ahumada[1] and GROWTH friends

[1] *Department of Astronomy, University of Maryland, College Park, MD 20742, USA*

ABSTRACT

The *Fermi* Gamma-ray Burst Monitor (GBM) detects ~ 40 short gamma-ray bursts (SGRBs) per year; however, their large localization regions have made the search for optical counterparts a challenging endeavour. We have developed and executed an extensive program with the wide field of view of the Zwicky Transient Facility (ZTF) camera, mounted on the Palomar 48 inch Oschin telescope (P48), to perform target-of-opportunity (ToO) observations on 11 *Fermi*-GBM SGRBs during 2018 and 2020-2021. Bridging the large sky areas with small field of view optical telescopes in order to track the evolution of potential candidates, we look for the elusive SGRB afterglow and kilonovae (KNe) associated with these high-energy events. Even though no counterpart has yet been found, more than 10 ground based telescopes, part of the Global Relay of Observatories Watching Transients Happen (GROWTH) network, have taken part in these efforts. The candidate selection procedure and the follow-up strategy have shown that ZTF is an efficient instrument for searching for poorly localized SGRBs, retrieving a reasonable number of candidates to follow-up and showing promising capabilities as the community approaches the multi-messenger era. Based on the median limiting magnitude of ZTF, our searches would have been able to retrieve a GW170817like event up to ~ 200 Mpc and SGRB afterglows to z = 0.2 or 0.4, depending on the assumed underlying energy model. Future TOOs will expand the horizon to z = 0.25 and 0.9 respectively.

1. INTRODUCTION

Between the years 1969–1972, analysis of the Vela Satellites' data confirmed the cosmic origin of gamma-ray detections (Klebesadel et al. 1973). These gamma-ray bursts (GRBs) are among the brightest events in the universe, and have been observed both in nearby galaxies as well as at cosmological distances (Metzger et al. 1997). The data collected over the years suggest a bimodal distribution in the time duration of the GRB that distinguishes two isotropically distributed groups: long GRBs (LGRB; $t_{90} > 2s$) and short GRBs (SGRB; $t_{90} < 2s$) (Kouveliotou et al. 1993), where t_{90} is defined as the duration that encloses the 5th to the 95th percentiles of the total counts in the energy range 20-2000 keV.

LGRBs have been associated with supernova (SN) explosions (Bloom et al. 1999; Woosley & Bloom 2006) and a large number of them have counterparts at lower wavelengths (Cano et al. 2017). On the other hand only ~ 35 SGRBs have optical/NIR detections (Fong et al. 2015; Rastinejad et al. 2021), thus their progenitors are still an active area of research. SGRBs have been shown to occur in environments with old populations of stars (Berger et al. 2005; D'Avanzo 2015) and have long been linked with mergers of compact binaries, such as binary neutron star (BNS) and neutron star–black hole (NSBH) (Narayan et al. 1992). The discovery of the gravitational wave event GW170817 coincident with the short gamma-ray burst GRB 170817A, unambiguously confirmed BNS mergers as at least one of the mechanisms that can produce a SGRB (Abbott et al. 2017a). However, compact binary mergers might not be the only source of SGRBs, as collapsars (Ahumada et al. 2021; Zhang et al. 2021) and giant flares from magnetars (Burns et al. 2021) can masquerade as short duration GRBs. Hence, the traditional classification of a burst based solely on the time duration is subject to debate (Zhang & Choi 2008; Bromberg et al. 2013; Amati 2021). For example, other gamma-ray properties (i.e. the hardness ratio) can cluster the bursts in different populations (Nakar 2007), and there are a couple of examples for which the time classification of the burst has been proven wrong due to the presence or lack of SN emissions (Gal-Yam et al. 2006; Ahumada et al. 2021; Zhang et al. 2021; Rossi et al. 2021). In this context, the search for the optical counterparts of SGRBs is essential to unveil the nature of their progenitors and the underlying physics.

Not all SGRBs show similar gamma-ray features and different models have tried to explain the observations. For example, the "fireball" model (Wijers et al. 1997;

Mészáros & Rees 1998) describes a highly relativistic jet of charged particle plasma emitted by a compact central engine as a result of a BNS or NSBH merger. The model predicts the production of gamma rays and hard X-rays within the jet. The interaction of the jet and the material surrounding the source produces emission in the X-ray, optical, and radio wavelengths. This "afterglow" lasts from days to months depending on the frequency range.

Different models have been applied to the observations that followed GW170817. Among the most popular is the classical case of a narrow and highly relativistic jet powered by a compact central engine (Goldstein et al. 2017). Deviations in the light-curves derived from classical models have motivated further developments (Willingale et al. 2007; Cannizzo & Gehrels 2009; Metzger et al. 2011; Duffell & MacFadyen 2015), including Gaussian structured jets (Kumar & Granot 2003; Abbott et al. 2017b; Troja et al. 2017) that can be detected off-axis and do not require the jet to point directly to Earth. Other models predict a more isotropic emission profile, produced by an expanding cocoon formed as the jet makes its way throughout the ejected material, reaching a Lorentz factor on the order of a few (Nagakura et al. 2014; Lazzati et al. 2017; Kasliwal et al. 2017; Mooley et al. 2017).

In addition to the GRB afterglow, in the event of a BNS or NSBH merger, the highly neutron rich material undergoes a rapid neutron capture (r-process), which creates heavy elements and enriches galaxies with rare metals (Côté et al. 2018). Some of the products of the r-process include highly radioactive elements; the decay of these newly created elements can energize the ejecta. The produced thermal radiation eventually powers a transient known as a *kilonova* (KN) (Lattimer & Schramm 1974; Li & Paczynski 1998; Metzger et al. 2010; Rosswog 2015; Kasen et al. 2017). Compared to the optical emission of an on-axis SGRB afterglow, a KN is expected to be orders of magnitude fainter. There have been attempts to separate the light of the SGRB afterglow and the KN (Fong et al. 2016; Troja et al. 2019; O'Connor et al. 2020; Fong et al. 2021), however this still presents a number of challenges.

Identifying optical counterparts to compact binary mergers can provide a rich scientific output, as demonstrated by the discovery of AT2017gfo (Chornock et al. 2017; Coulter et al. 2017; Cowperthwaite et al. 2017a; Drout et al. 2017; Evans et al. 2017; Kasliwal et al. 2017; Kilpatrick et al. 2017; Lipunov et al. 2017; McCully et al. 2017; Nicholl et al. 2017; Shappee et al. 2017; Pian et al. 2017; Smartt et al. 2017) which led to discoveries in areas as diverse as r-process nucleosynthesis, jet physics, host galaxy properties, and even cosmology (Kasliwal et al. 2017; Arcavi et al. 2017; Tanvir et al. 2017; Chornock et al. 2017; Cowperthwaite et al. 2017b; Drout et al. 2017; Kasen et al. 2017; Pian et al. 2017; Smartt et al. 2017; Troja et al. 2017). Previous studies have used the arcminute localizations achieved with the *Swift* Burst Alert Telescope (BAT) to find and characterize SGRBs optical counterparts (Fong et al. 2015; Rastinejad et al. 2021), however the number of associations is still a few dozens. Others have tried following-up thousands of square degrees of the LIGO-Virgo Collaboration (LVC) maps (Coughlin et al. 2019a,b; Andreoni et al. 2019; Goldstein et al. 2019; Andreoni et al. 2020; Hosseinzadeh et al. 2019; Vieira et al. 2020; Anand et al. 2020; Kasliwal et al. 2020) in the hopes of localizing EM counterparts to gravitational wave events, to no avail. Moreover, other studies have tried to serendipitously find the elusive KN (Chatterjee et al. 2019; Andreoni et al. 2020, 2021), but they have so far only been able to constrain the local rate of compact binary mergers using wide field of view (FOV) synoptic surveys.

In this paper we present a summary of the systematic and dedicated optical search of Fermi-GMB SGRBs using the Palomar 48-inch telescope equipped with the 47 square degree ZTF camera over the course of 2 years. Previous studies (Singer et al. 2013, 2015) have successfully found optical counterparts to *Fermi*-GBM LGRBs using the intermediate Palomar Transient Factory (iPTF) (Law et al. 2009; Rau et al. 2009), and other ongoing projects like Global MASTER-Net (Lipunov et al. 2005), the Nordic Optical Telescope (NOT; Djupvik & Andersen (2010)) and the Gravitational-Wave Optical Transient Observe (GOTO; Mong et al. (2021)) are using optical telescopes to scan the large regions derived by GBM. We note that the optical afterglows of LGRBs are usually brighter than of SGRBs, thus the ToO strategy might differ from the one presented in this paper. We base our triggers on GBM events since GBM is more sensitive to higher energies than *Swift* and it detects SGRBs at four times the rate of *Swift*, making it the most prolific compact binary merger detector.

In section 2 we describe the facilities involved along with the observations and data taken during the campaign. We describe our filtering criteria and how candidates are selected and followed up in section 3, and detail the *Fermi* events we followed up in section 4. In section 5 we compare our observational limits to SGRB transients in the literature. In section 6 we discuss the implications of the optical non-detection of a source and we explore the sensitivity of our searches. Using the lightcurves of the transients generated for our efficiency analysis, we put the detection of an optical counterpart in context for future ToO follow-up efforts in section 7 We summarize our work in section 8.

2. OBSERVATIONS AND DATA

In this section we will broadly describe the characteristics of the telescopes and instruments involved in this campaign, as well as the observations. We start with the *Fermi*-GBM, our unique source of compact mergers, followed by ZTF, our transient discovery engine, and finally describe the facilities used for detailed follow-up.

2.1. *Fermi Gamma-ray Burst Monitor*

The Gamma-ray Burst Monitor (GBM) is an instrument on board the *Fermi* Gamma-ray Space Telescope sensitive to gamma-ray photons with energies from 8 keV to 40 MeV (Meegan et al. 2009). The average rest frame energy peak for SGRBs ($E_{p,i} \sim 0.5$ MeV; Zhang et al. (2012)) is enclosed in the observable GBM energy range and not in the Swift BAT energy range (5-150 KeV). Additionally, any given burst should be seen by a number of detectors, as GBM is sensitive to gamma-rays from the entire unocculted sky.

The low local rate of Swift SGRBs has impeded the discovery of more GW170817-like transients (Dichiara et al. 2020). On the other hand, GBM detects close to 40 SGRBs (Meegan et al. 2009) per year, four times the rate of Swift. However, the localization regions given by GBM usually span a large portion of the sky, going from a few hundreds sq. degrees to even a few thousands sq. degrees. The median of 283 sq. deg (von Kienlin et al. 2020) makes the systematic search for counterparts technically challenging and time consuming.

The adopted strategy prioritizes *Fermi*-GBM SGRBs events visible from Palomar that present a hard spike followed by a soft thermal tail, similar to GRB 170817A (Goldstein et al. 2017). During the second half of our campaign, we restricted our triggers to the events for which more than 75% of the error region could be covered twice in ∼2 hrs. With ZTF this corresponds to a requirement that 75% of the map encloses less than 500 sq deg. In Table 1 a few features of the SGRBs selected for follow-up are listed.

2.2. *The Zwicky Transient Facility*

We have used ZTF to scan the localization regions derived by the *Fermi*-GBM. ZTF is a public-private project in the time domain realm which employs a dedicated camera on the Palomar 48-inch Schmidt telescope. The ZTF field of view is 47 deg^2, which usually allows us to observe more than 50% of the SGRB error region in less than one night. The public ZTF survey covers the observable northern sky every two nights in g- and r-bands with an standard exposure time of 30 s, reaching an average 5σ detection limit of $r = 20.6$ (Graham et al. 2019a; Bellm et al. 2018).

Two ToO strategies were tested during this campaign, one during 2018 and the second during 2020-2021. Most modifications came after lessons learned during the follow-up efforts of gravitational waves in 2019 (Coughlin et al. 2019b; Anand et al. 2020; Kasliwal et al. 2020). The original ToO observing plan allowed us to start up to 36 hrs from the SGRB GBM trigger. However, since the afterglow we expect is already faint ($m_r > 19$ mag) and fast fading ($\Delta m/\Delta t > 0.3$ mag per day), our revised strategy only includes triggers that can be observed from Palomar within 12 hrs. The exposure time for each trigger ranges from 60 s to 300 s depending on the size of the localization, as there is a trade-off between exposure time and coverage. We generally prioritized coverage over depth, and for the second half of our campaign, we only triggered on maps where more than 75% of the region could be covered. The same sequence is repeated a second time the following night, unless additional information from other spacecraft modifies the error region. Generally, fields with an airmass > 2.5 are removed from the observing plan.

We schedule two to three sets of observations depending on the visibility of the region, using the ZTF r- and g-bands. The combination of r- and g-band observations was motivated by the need to look for afterglows and KNe, which are both fast evolving red transients. In fact, the SGRB afterglows in the literature show red colors (i.e. $g - r > 0.3$) and a rapid evolution, fading faster than $\Delta m_r/\Delta t > 0.5$ mag per day. On the other hand, GW170817 started off with bluer colors and evolved dramatically fast in the optical during the first days, with $g - r = 0.5$ mag 1 day after the *Fermi* alert and $\Delta m_g/\Delta t > 1$ mag per day. Even though we expect a fast fading transient, if we assume conservative fading rates of 0.3-0.5 mag per day, we would need observations separated by 8 to 5 hrs to detect the decline using ZTF data with errors of the order of 0.1 mag. This ToO strategy thus relies on the color of transients for candidate discrimination, as this is easier to schedule than multi-epoch single-band photometry within the same night and with sufficient spacing between observations.

We followed up on 10 *Fermi*-GBM SGRBs, their skymaps and the corresponding ZTF footprints are shown in Figures 1, 2, and 3. As listed in Table 1, all of the events span more than 100 deg^2, which is the average localization covered during previous LGRBs searches (Singer et al. 2015). Moreover, in many cases,

GRB	Fermi Trigger	Time [JD]	t_{90} [s]	90% C.R. Area	50% C.R. Area	S/N	E_{peak} $[keV]$
GRB 180523B	548793993	2458262.2823	1.984	5094 deg^2	852 deg^2	6.9.	1430 ± 687
GRB 180626C	551697835	2458295.8916	0.960	5509 deg^2	349 deg^2	7.1.	446 ± 98
GRB 180715B	553369644	2458315.2412	1.664	4383 deg^2	192 deg^2	12.5	559 ± 112
GRB 180728B	554505003	2458328.3819	0.832	397 deg^2	47 deg^2	20.2	504 ± 61
GRB 180913A	558557292	2458375.2834	0.768	3951 deg^2	216 deg^2	10.0	444 ± 175
GRB 181126B	564897175	2458448.6617	1.664	3785 deg^2	356 deg^2	7.5	1049 ± 241
GRB 200514B	611140062	2458983.8802	1.664	590 deg^2	173 deg^2	5.1	†
GRB 201130A	628407054	2459183.7297	1.280	545 deg^2	139 deg^2	5.3	†
GRB 210510A	642367205	2459345.3055	1.344	1170 deg^2	343 deg^2	5.6	194 ± 60
GRB 210529B	644025222	2459364.1773	2.368	434 deg^2	114 deg^2	6.0	240 ± 78

Table 1. Global features of the *Fermi*-GBM SGRB followed-up with ZTF. The peak energies come from the public Fermi catalog for GRB 180523B, GRB 180626C, GRB 180715B, GRB 180913A and GRB 181126B. Additionally, we compiled E_p listed in Hamburg et al. 2018 for GRB 180728B, and analyzed GRB 200514B, GRB 201130A, GRB 210510A, GRB 210529B independently. We list the GRB name, their trigger number, the Julian day (JD) of each event, the t_{90} duration, the area encompassed by the 90% and 50% credible region (C.R.), the signal-to-noise ratio from the Fermi detection and the peak energy of the gamma-ray spectrum (E_{peak}). For events with a †, the power law model is preferred over the comptonized model, thus there is no E_p parameter. We exclude from this list the parameters of GRB 200826A, as it was not related to a compact binary merger.

the 90% credible region (C.R.) spans more than 1000 deg^2, which is challenging even for a 47 deg^2 field of view instrument such as ZTF.

Triggering ToO observations for survey instruments like ZTF and Palomar Gattini-IR (De et al. 2020) halts their ongoing survey observations and redirects them to observe only certain fields as directed by an observation plan. We have used `gwemopt` (Coughlin et al. 2018, 2019a), a code intended to optimize targeted observations for gravitational wave events, to achieve an efficient schedule for our ToO observations. The similarities between LVC and GBM skymaps allow us to apply the same algorithm, which involves slicing the skymap into the predefined ZTF tiles and determining the optimal schedule by taking into consideration the observability windows and the need for a repeated exposure of the fields. In order to prioritize the fields with the highest enclosed probability, we used the "greedy" algorithm described in Almualla et al. (2020). As `gwemopt` handles both synoptic and galaxy-targeted search strategies; we employed the former to conduct observations with some of our facilities, Palomar Gattini-IR, GROWTH-India and ZTF, and the latter for scheduling observations with the Kitt Peak EMCCD Demonstrator (KPED; Coughlin et al. 2019b).

2.3. *Optical follow-up*

Following the identification of candidate counterparts with ZTF, subsequent optical follow-up of these transients is required to classify them. For the candidates that met the requirements described in Section 3, mainly meaning they showed interesting light-curve history and magnitude evolution, we acquired additional data. To obtain these data, the GROWTH multi-messenger group relies on a number of telescopes around the globe. Most of these facilities are strategically located in the Northern Hemisphere, enabling continuous follow-up of ZTF sources. The follow-up observations included both photometric and spectroscopic observations. Even though the spectroscopic classification is preferable, photometry was essential to rule out transients, based on their color evolution and fading rates. The telescopes involved in the photometric and spectroscopic monitoring are briefly described in the following paragraphs.

We used the Kitt Peak Electron multiplying CCD Demonstrator (KPED) on the Kitt Peak 84 inch telescope (Coughlin et al. 2019b) to obtain photometric data. The KPED is a fairly new instrument which has been used as a single-band optical detector in the Sloan g- and r- bands and Johnson *UVRI* filters and it is mounted on a fully roboticized telescope. The FOV is $4.4' \times 4.4'$ and the pixel size is $0.259''$.

Each candidate scheduled for photometry was observed in the g- and r- band for 300 s. The data taken with KPED is then dark subtracted and flat-field calibrated. After applying astrometric corrections, the instrumental magnitudes were determined using Source Extractor (Bertin, E. & Arnouts, S. 1996). To calculate the apparent magnitude of the candidate, the zero-point

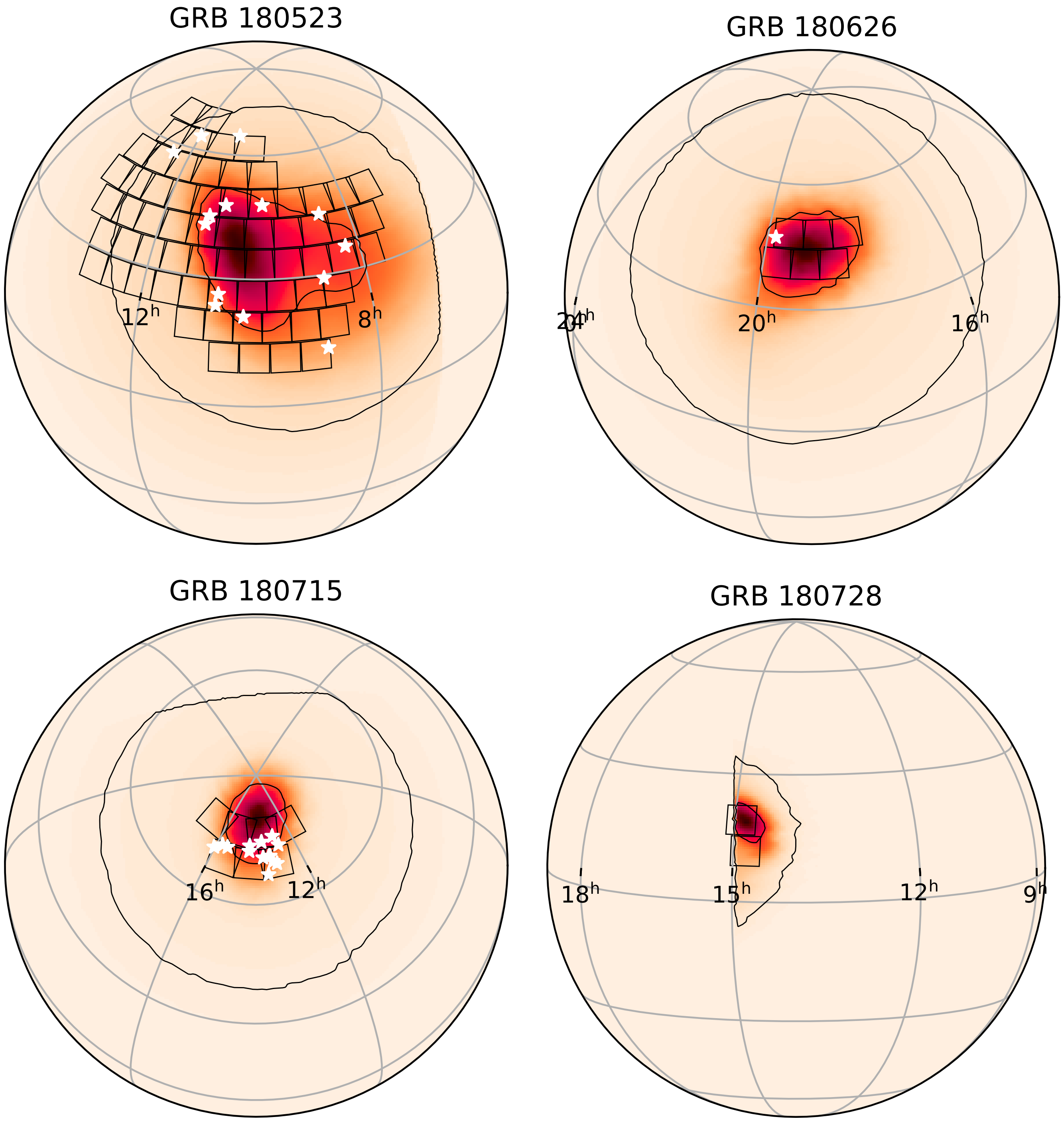
GRB 180523

GRB 180626

GRB 180715

GRB 180728

Figure 1. Coverage of four ZTF triggers on Fermi GBM regions. Starting on the top left, the skymaps of GRB 180523, GRB 180626, GRB 180715, and GRB 180728 are shown along the ≈ 47 deg^2 ZTF tiles (black quadrilaterals). The 50% and 90% credible regions are shown as black countours and the sources discovered during the ZTF trigger as white stars (described in Table 4-7).

of the field is calibrated using Pan-STARRS 1 (PS1) and Sloan Digital Sky Survey (SDSS) stars in the field as standards. Given the coordinates of the target, an on-the-fly query to PAN-STARRS1 and SDSS retrieves the stars within the field that have a minimum of 4 detections in each band.

Additionally, sources were photometrically followed-up using the Las Cumbres Observatory Global Telescope (LCOGT) (PI: Coughlin, Andreoni) (Brown et al. 2013). We used the 1-m and 2-m telescopes to scheduled sets of 300 s in the g-, r- and i-band. The LCOGT data comes already processed and in order to determine the magnitude of the transient, the same PS1/SDSS cross-matching strategy used for KPED was implemented for LCOGT images.

We used the Spectral Energy Distribution Machine (SEDM) on the Palomar 60-inch telescope (Blagorodnova et al. 2018) to acquire g-, r-, and i- band imaging with the Rainbow Camera on SEDM in 300 s exposures. Images were then processed using a python-based pipeline that performs standard photometric reduction techniques and uses an adaptation of `FPipe` (Fremling Automated Pipeline; described in detail in Fremling et al. (2016)) for difference imaging. Moreover, we employed the Integral Field Unit (IFU) on SEDM, a robotic spectrograph on the Palomar 60-inch telescope (Blagorodnova et al. 2018) to observe targets brighter than $m_{AB} < 19$ mag. Each observation is reduced and calibrated using the `pysedm` pipeline Rigault et al. (2019), which applies standard calibrations using standards taken during the observing night. Once the spectra is extracted we use the `SuperNova IDentification`[1] software (`SNID`; Blondin & Tonry 2007) for spectroscopic classification.

We obtained spectra for six candidates using the Double Spectrograph (DBSP) on the Palomar 200-inch telescope during classical observing runs. The data was taken using the 1.5″slit and reduced following a custom PyRAF pipeline [2] (Bellm & Sesar 2016).

The other telescopes used for photometric follow-up are the GROWTH India telescope (GIT) in Hanle, India, the Liverpool Telescope (Steele et al. 2004) in La Palma, Spain, and the Akeno telescope (Kotani et al. 2007) in Japan. The requested observations in the g-, r- and i-band varied between 300s and 600s depending on the telescope.

We obtained spectra with the DeVeny Spectrograph at the Lowell Discovery Telescope (LDT) (MacFarlane & Dunham 2004) and the 10m Keck Low Resolution Imaging Spectrograph (LRIS) (Oke et al. 1995). We reduced these spectra with PyRAF following standard long-slit reduction methods.

We used the Gemini Multi-Object Spectrograph (GMOS-N) mounted on the Gemini-North 8-meter telescope on Mauna Kea to obtain photometric and spectroscopic data (P.I. Ahumada, GN-2021A-Q-102). Our standard photometric epochs consisted on four 180s exposures in r-band to measure the fading rate of the candidates, although we included g-band when the color was relevant. These images were processed using DRAGONS (Labrie et al. 2019) and the magnitudes were derived after calibrating against PS1. When necessary and possible, we used PS1 references to subtract the host, using HOTPANTS. For spectroscopic data, our standard was four 650 s exposures using the 1” long-slit and the R400 grating and we used PyRAF standard reduction techniques to reduce the data.

3. CANDIDATES

After a given ZTF observation finishes, the resulting image is subtracted to a reference image of the field. The latter process involves a refined PSF adjustment and a precise image alignment in order to perform the subtraction and determine flux residuals. Any 5σ difference in brightness creates an ‘*alert*’ (Graham et al. 2019b; Masci et al. 2019), a package with information describing the transient. The alerts include the magnitude of the transient, proximity to other sources and its previous history of detections among other features.ZTF generates around 10^5 alerts per night of observation, which corresponds to $\sim 10\%$ of the estimated Vera Rubin observatory alert rate. The procedure to reduce the number of alerts from $\sim 10^5$ to a handful of potential optical SGRB counterparts is described in this section.

In general terms, the method involves an rigid online alert filtering scheme that significantly reduces the number of sources based on image quality features. Then, the selection of candidates takes into consideration the physical properties of the transient (i.e. cross-matching with AGN and solar system objects), as well as archival observations from different surveys. After visually inspecting the candidates that passed the preliminary filters, scientists in the collaboration proceed to select sources based on their light-curves, color and other features (i.e. proximity to a potential host, redshift of the host, etc.). This method allows to recover objects that are later scheduled for further follow-up.

The candidate selection and the follow-up are coordinated via the GROWTH marshal (Kasliwal et al. 2018) and lately through the open-source platform and alert

---

[1] https://people.lam.fr/blondin.stephane/software/SNID/

[2] https://github.com/ebellm/pyraf-dbsp

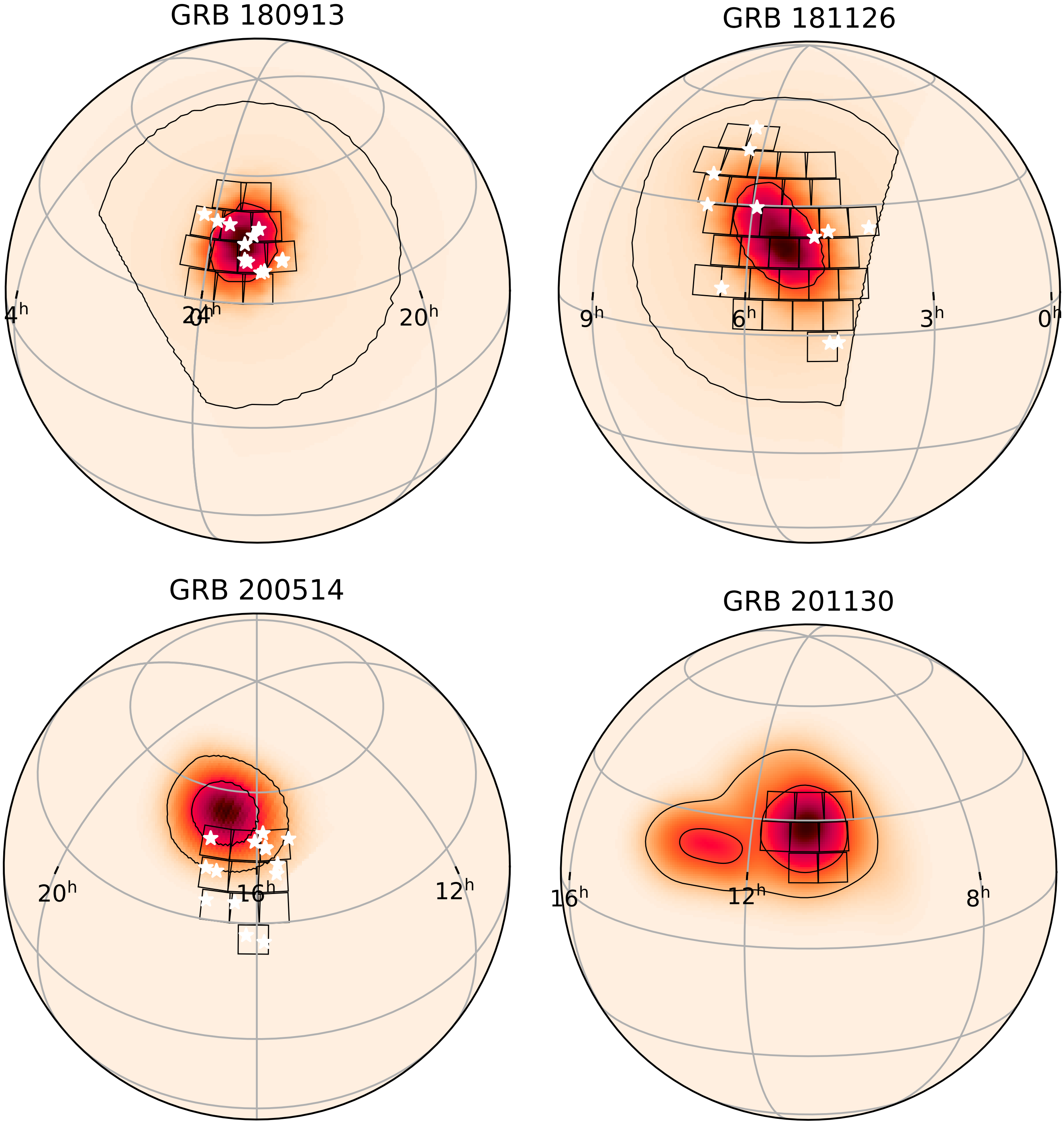

Figure 2. Coverage of the six ZTF triggers on Fermi GBM regions. From top to bottom and left to right, the skymaps of GRB 180913, GRB 181126, GRB 200514, and GRB 201130 are shown along the ≈ 47 deg^2 ZTF tiles (black quadrilaterals). The 50% and 90% credible regions are shown as black countours and the sources discovered during the ZTFtrigger as white stars (described in Table 7-**??**).

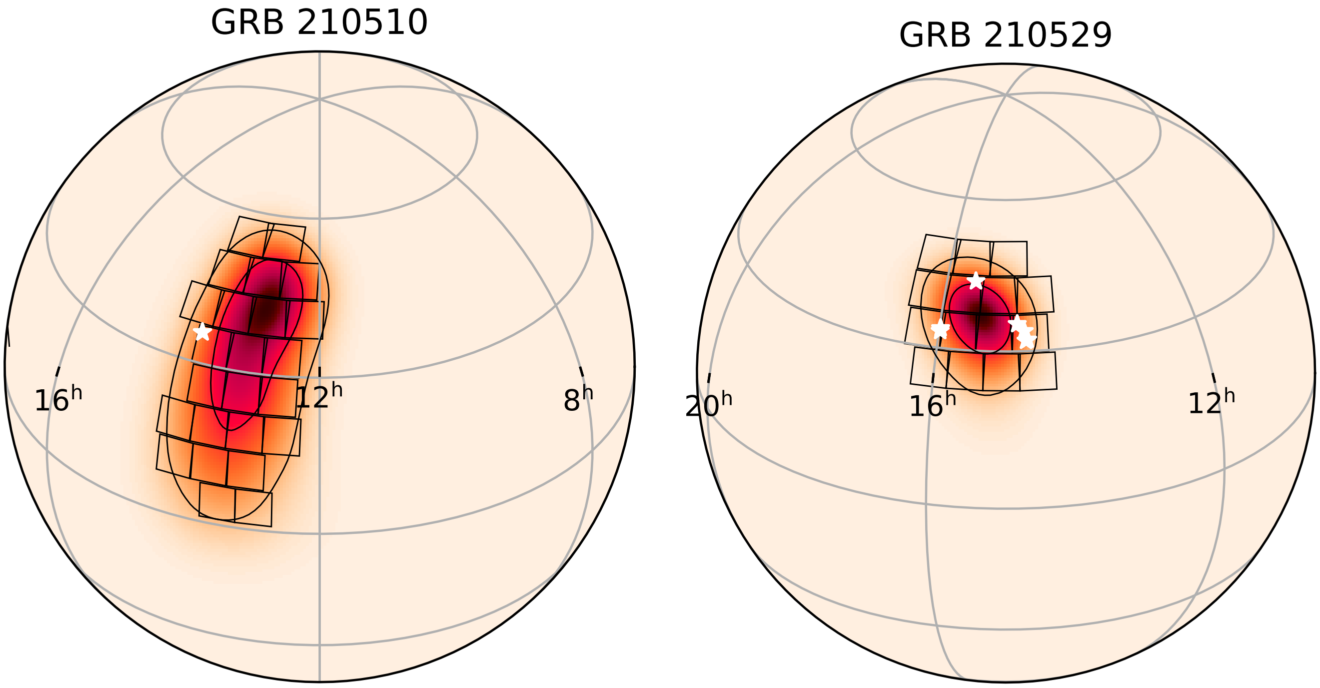

Figure 3. Coverage of the six ZTF triggers on Fermi GBM regions. From top to bottom and left to right, the skymaps of GRB 210510, and GRB 210529 are shown along the ≈ 47 deg^2 ZTF tiles (black quadrilaterals). The 50% and 90% credible regions are shown as black countours and the sources discovered during the ZTFtrigger as white stars (described in Table 10-11).

broker Fritz[3]. A summary of the numbers of followed-up objects for each trigger is in Table 3 and the details of the filtering scheme are described below. It is worth mentioning than more than 3×10^5 alerts were generated during the 10 ToO triggers, while ∼80 objects were circulated in the Gamma-ray Coordinates Network (GCN).

3.1. *Detection and filtering*

In the searches for the optical counterpart for SGRBs, we query the ZTF data stream using the GROWTH marshal (Kasliwal et al. 2018), the `Kowalski` infrastructure (Duev et al. 2019)[4], he `NuZTF` pipeline (Stein et al. 2021; Stein et al. 2021) built using `Ampel` (Nordin et al. 2019) [5], and Fritz. The filtering scheme restricted the transients to those with the following properties:

- **Within the skymap:** To ensure the candidates are in the GBM skymap, we implemented a cone search in the GBM region with `Kowalski` and `Ampel`. With the GROWTH marshal approach, we retrieve only the candidates in the fields scheduled for ToO. We note that a more refined analysis on the coordinates of the candidates is done after this automatic selection.

- **Positive subtraction:** After the new image is subtracted, we filter on the sources with a positive residual, thus the ones that have brightened.

- **It is real:** To distinguish sources that are created by ghosts or artifacts in the CCDs, we apply a random-forest model (Mahabal et al. 2019) that was trained with common artifacts found in the ZTF images. We restrict the Real-Bogus score to > 0.25 as it best separates the two populations. For observations that occurred after 2019, we used the improved deep learning real-bogus score `drb` and we set the threshold to sources with `drb` score > 0.15 (Duev et al. 2019).

- **No point source underneath:** To rule out stellar variability we require the transient to have a separation of 3″ from any point source in the PS1 catalog based on Tachibana & Miller (2018).

- **Two detections:** We require a minimum of two detections separated by at least 30 min. This allows us to reject cosmic rays and moving solar system objects.

---

[3] https://github.com/fritz-marshal/fritz

[4] https://github.com/dmitryduev/kowalski

[5] https://github.com/AmpelProject

- **Far from a bright star:** To further avoid ghosts and artifacts, we require the transient to be $>20''$ from any bright ($m_{\rm AB} < 15$ mag) star.

- **No previous history:** As we do not expect the optical counterpart of a SGRB to be a periodic variable source, we restrict our selection to only the sources that are detected after the event time and have no alerts generated for dates prior to the GRB.

As a reference, this first filtering step reduced the total number of sources to a median of $\sim 0.04\%$ of the original number of alerts.

3.2. *Scanning and selection*

Generally, after the first filter step, the number of transients is reduced to a manageable amount. These candidates are then cross-matched with public all-sky surveys such as Wide-field Infrared Survey Explorer (WISE; Cutri et al. 2013), Pan-STARRS 1 (PS1; Chambers et al. 2016), Sloan Digital Sky Survey (SDSS; Ahumada et al. 2020a), the Catalina Real-time Transient Survey (CRTS; Djorgovski et al. 2011),and Asteroid Terrestrial-impact Last Alert System (ATLAS; Tonry 2011). We use the WISE colors to rule out candidates, as active galactic nuclei (AGN) are located in a particular region in the WISE color space (Wright et al. 2010; Stern et al. 2012). If a candidate has a previous detection in ATLAS or has been reported to Transient Name Server (TNS) before the event time it is also removed from the candidate list. We additionally cross-match the position of the candidates with the Minor Planet Center (MPC) to rule out any other slow moving object. We use the PS1 DR2 [6] to query single detections at the location of the transients, and we use this infomation to rule out sources based on serendipitous previous activity.

One of the most important steps in our selection of transients is the rejection of sources using forced photometry (FP) on ZTF images. For this purpose we run two FP pipelines: ForcePhotZTF[7] (Yao et al. 2019) and the ZTF FP pipeline (Masci et al. 2019). We limit our search to a 100 days before the burst and reject sources with consistent $\geq 4\sigma$ detections.

Finally, we manually scan and vet candidates passing those cuts, referring to cutouts of the science images, photometric decay rates, and color evolution information in order to select the most promising candidates.

A detailed table with the candidates discovered by ZTF for the SGRB campaign are shown in Tables 4-8.

3.3. *Rejection Criteria*

In order to find an optical counterpart, further monitoring of the discovered transients is needed. We have taken spectra for the most promising candidates to classify them. Most of the spectra acquired correspond to bright SNe (as in Figure 5) and a few re-discovered Cataclysmic Variables (CVs). After the 10 SGRBs follow-ups, we obtained 19 spectra, however none of them has exhibited KN features. We have used the 'Deep Learning for the Automated Spectral Classification of Supernovae and Their Hosts' or `dash` (Muthukrishna et al. 2019) to determine the classification of the candidates with SNe spectral features. CVs were recognized as they show H features at redshift $z = 0$.

For the sources that do not have spectra available, we monitored their photometric evolution with the facilities described in Section 2. Even though the photometric classification cannot be entirely conclusive, there are characteristic features shared between afterglows and KNe. On one side, afterglows are known to follow a power-law decay of the form $F \sim t^{-\alpha}$. On the other hand, KN models (Bulla 2019) show that most parameters will evolve faster then 0.3 mag per day (i.e. $\Delta m/\Delta t > 0.3$ mag; Anand et al. (2020)). As a reference, GW170817 faded over ~ 1 mag over the course of 3 days and other SGRB optical counterparts have shown a rapid magnitude evolution as well (Fong et al. 2015; Rastinejad et al. 2021). The astrophysical events that most contaminated our sample are SNe, but they normally show a monotonic increase in their brightness during their first tens of days, to later decay at a slower rate than expected for afterglows or KNe. Other objects like slow-moving asteroids and flares are less common and can be removed inspecting the images or performing a detailed archival search in ZTF and other surveys.

To illustrate the photometric rejection, we show two transients in Fig. 4 with no previous activity in the ZTF archives previous to the SGRB. As their magnitude evolution in both r- and g- band does not pass our threshold, we conclude they are not related to the event. This process was repeated for all candidates without spectral information, using all the available photometric data in ZTF and partner telescopes.

4. SGRB EVENTS

4.1. *GRB 180523B*

The first set of ToO observations of this program was taken 9.1 hours after GRB 180523B (trigger 548793993). We covered ~ 2900 deg^2, which corresponds to 60% of

---

[6] https://catalogs.mast.stsci.edu/panstarrs/

[7] https://github.com/yaoyuhan/ForcePhotZTF

GRB	SNR>5	Positive subtraction	Real	Not star underneath	Far from bright star	Two detections	Circulated in GCNs
GRB 180523B	67614	17374	12117	687	669	297	14
GRB 180626C	10602	5040	4967	1582	1377	214	1
GRB 180715B	33064	7611	7515	6941	5509	104	14
GRB 180728B	18488	1450	1428	859	739	51	7
GRB 180913A	25913	12105	12077	6284	5145	372	12
GRB 181126B	40342	30455	30416	22759	21769	340	11
GRB 200514B	20610	10983	10602	4502	4422	1346	14
GRB 200826A	13488	8142	7744	3892	3785	464	14
GRB 201130A	1972	1045	990	647	637	43	0
GRB 210510A	41683	27229	28940	16977	16973	1562	1
GRB 210529B	26778	15942	15109	7185	1085	1253	7
	Median reduction	52.99%	50.2%	24.25 %	19.86%	2.02%	0.04%

Table 2. Summary of efficiency of our vetting strategy. For each GRB we list the number of alerts that survives after a given filtering step. The first column (SNA>5) shows the total number of alerts in the GRB map. The next columns show the number of alerts that show an increase in flux (Positive subtraction) and the real source, based on the real-bogus (RB) and `drb` scores. We set the thresholds to RB>0.25 and `drb`>0.5. The next columns show the number of sources that are not related to a point source, nor close to a bright star, to avoid artifacts. To avoid moving objects, we show the number of sources with two detections separated by at least 30 min. The last column shows the number of sources we circulated as potential candidates for each trigger. For each step, we calculate the median reduction of alerts and list this number at the end of each column.

the localization region after accounting for chip gaps in the instrument (Coughlin et al. 2018b). The median 5 sigma upper limit for an isolated point source in our images was $r > 20.3$ mag and $g > 20.6$ mag and after 2 days of observations we arrived at 14 viable candidates that required follow-up. We were able to spectroscopically classify 4 transients as SNe and photometrically follow-up sources with KPED to determine that the magnitude evolution was slower than our threshold of $\Delta m/\Delta t > 0.3$ mag. This effort was summarized in Coughlin et al. (2019a) and the list of transients discovered is displayed in Table 4.

4.2. *GRB 180626C*

The SGRB GRB 180626C (*Fermi* trigger 551697835) came in the middle of the night at Palomar. We started observing after 1.5 hours and we were able to cover 275 $\deg^2$ of the GBM region. The localization, and hence the observing plan, was later updated as the region of interest was now the overlap between the *Fermi* and newly arrived InterPlanetary Network (IPN)[8] map. The observations covered finally 230 $\deg^2$, corresponding to the 87% of the intersecting region. After two nights of observations, with a median 5-sigma upper limit of $r > 21.1$ mag and $g > 21.0$ mag, only one candidate was found to have no previous history of evolution and be spatially coincident with the SGRB (Coughlin et al. 2018a).

The transient ZTF18aauebur was a rapidly evolving transient that faded from $g = 18.4$ to $g = 20.5$ in 1.92 days. This rapid evolution continued during the following months, fluctuating between $r \sim 18$ mag and $r \sim 19$ mag. It was interpreted as a stellar flare, as it is located close to the galactic plane and there is an underlying source in the PS1 and Galaxy Evolution Explorer (GALEX) (Morrissey et al. 2007) archive. Additionally, its SEDM spectrum showed a featureless blue spectrum and H-α absorption features at redshift $z = 0$, so it is an unrelated galactic source.

4.3. *GRB 180715B*

We triggered ToO observations to follow-up GRB 180715B (trigger 553369644) 10.3 hours after the GBM detection. We managed to observe $\sim 36\%$ of the localization region which translates into 254 $\deg^2$. The median limiting magnitude for these observations was of $r > 21.4$ mag and $g > 21.3$ mag.

During this campaign, we discovered 14 new transients (Cenko et al. 2018) in the region of interest. We were able to spectroscopically classify 2 candidates using instruments at the robotic Palomar 60 inch telescope (P60) and Palomar 200 inch Hale telescope (P200). The SEDM spectrum of ZTF18aauhpyb showed a stellar

---

[8] http://www.ssl.berkeley.edu/ipn3/index.html

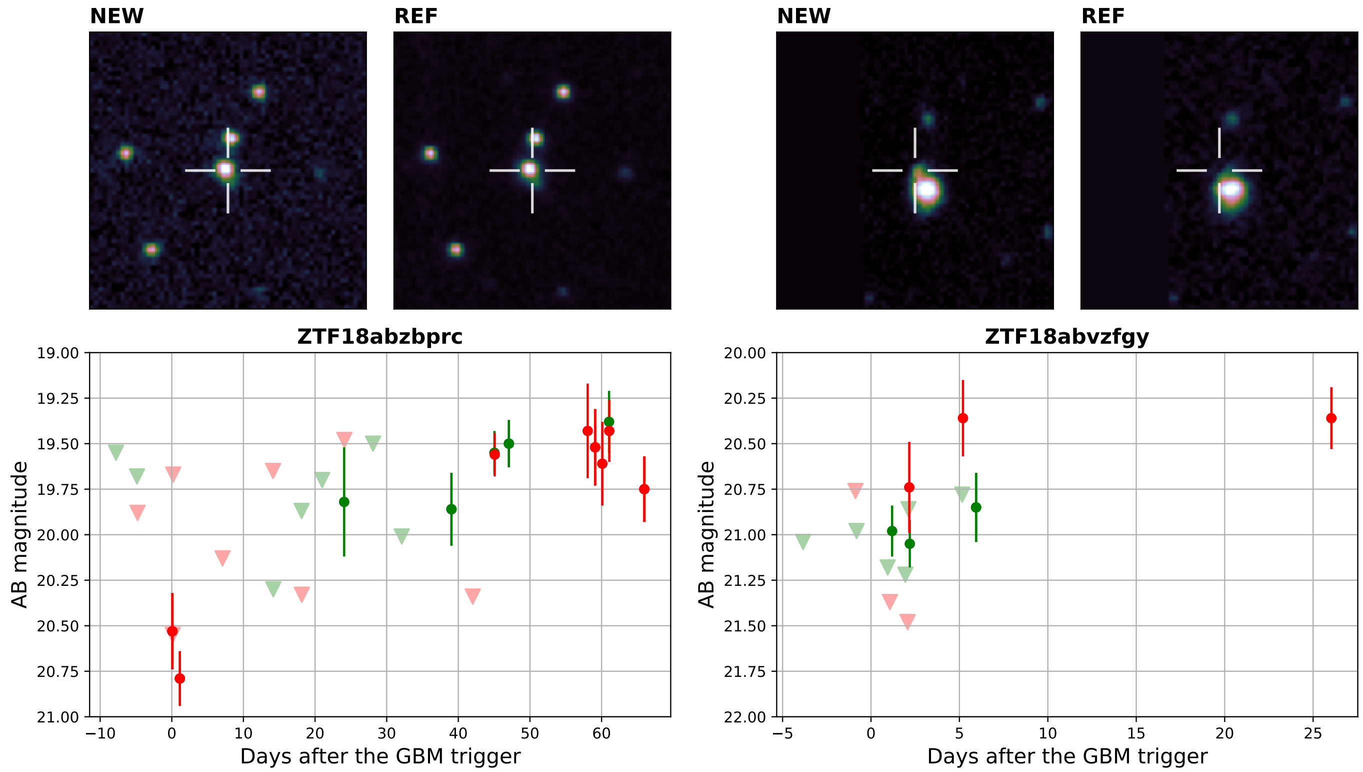

Figure 4. The light-curves for the promising candidates ZTF18abzbprc and ZTF18abvzfgy. The dotted line shows the Julian day of the GRB detection. The observations in g and r band are plotted in green and red colors respectively and the upper limits of non-detections are shown as triangles in the light-curve. Filled circles and filled squares represent ZTF and KPED data respectively.

source with H-Balmer features at redshift z = 0 and a blue continuum. The DBSP spectrum of ZTF18abhbfqf was best fitted by a SN Ia-91T. We show the rejection criteria used to rule-out associations with the SGRB in Table 6. Generally, most candidates showed a slow magnitude evolution (our threshold is $\Delta m/\Delta t > 0.3$ mag). Furthermore, three candidates (ZTF18abhhjyd, ZTF18abhbfoi and ZTF18abhawjn) matched with an AGN in the Milliquas (Flesch 2019) catalog. A summary of the candidates can be found in Table 6.

4.4. *GRB 180728B*

The follow-up ToO observations of the GRB 180728B (trigger 554505003) started ∼ 8 hours after the *Fermi* alert, however, it did not cover the later updated IPN localization. The following night and 31 hours after the *Fermi* detection we managed to observe the joint GBM and IPN localization, covering 334 deg^2 and ∼ 76% of the error region. The median upper limits for the scheduled observations were of r > 18.7 mag and g > 20.0 mag (Coughlin et al. 2018a). As a result of these observations, no new transients were found.

4.5. *GRB 180913A*

We triggered ToO observations with ZTF to follow-up the *Fermi* event GRB 180913A (trigger 558557292) about ∼ 8 hours after the detection. The first night of observations covered 546 deg^2. The schedule was adjusted as the localization improved once the IPN map was available. During the second night we covered 53% of the localization, translated into 403 deg^2. After a third night of observations, 12 transients were discovered and circulated in Coughlin et al. (2018b). The median upper limits for this set of observations were of r > 21.9 and g > 22.1 mag.

We obtained a spectrum of ZTF18abvzfgy with LDT, a fast rising transient ($\Delta m/\Delta t \sim 0.2$ mag per day) in the outskirts of a potential host. It was classified as a SN Ic-BL at a redshift of z = 0.04. The rest of the transients were follow-up photometrically with KPED and LCO, but generally showed a flat evolution. The candidate ZTF18abvzsld had previous PS1 detections, thus ruling it out as potential variable stellar sources. The rest of the candidates are listed in Table 7.

4.6. *GRB 181126B*

The last SGRB we follow-up before the start of the 2019 O3 LIGO/Virgo observing run was of the *Fermi*-

GBM event GRB 181126B (trigger 564897175). As this event came during the night at the ZTF site, the observations started $\sim$ 1.3 hours after the *Fermi* alert, and we were able to cover 1400 $\deg^2$, close to 66% of the GBM localization. After the IPN localization was available the next day, the observations were adjusted and we used ZTF to cover 709 $\deg^2$ and $\sim$ 76% of the overlapped region. The mean limiting magnitude of the observations were of $r > 20.8$ mag (Ahumada et al. 2018). After processing the data, we discovered 11 new optical transients timely and spatially coincident with the SGRB event. We took spectra of 7 of them with the Keck LRIS, discovering 6 SNe (ZTF18acrkkpc, ZTF18aadwfrc, ZTF18acrfond, ZTF18acrfymv, ZTF18acptgzz, ZTF18acrewzd) and 1 stellar flare (ZTF18acrkcxa). All of the candidates are listed in Table 8, and none of them showed rapid evolution.

4.7. *GRB 200514B*

We resumed the search for SGRB counterparts with ZTF once LIGO/Virgo finished O3. On 2020-05-14 we used ZTF to cover over 519.3 $\deg^2$ of the error region of GRB 200514B (trigger 611140062). These corresponded roughly to $\sim$ 50% of the error region. After the first night of observations, 7 candidates passed our filters and were later circulated in Ahumada et al. (2020). The observations during the following night resulted in 7 additional candidates (Reusch et al. 2020a). The depth of these observations reached 22.4 and 22.2 mag in the g- and r-band respectively. After IPN released their analysis (Svinkin et al. 2020), 9 of our candidates remained in the localization region. Our follow-up with ZTF and LCO showed that none of these transients evolved as fast as expected for a GRB afterglow (see Table 9).

4.8. *GRB 200826A*

This burst is described extensively in Ahumada et al. (2021), as well as in other works (Zhang et al. 2021; Rossi et al. 2021; Rhodes et al. 2021). It was the only short duration GRB in our campaign with an optical counterpart association. However, despite its short duration (t_{90}=1.13s), it showed a photometric bump in the i-band that could only be explained by an underlying SN (Ahumada et al. 2020,b). This makes GRB 200826A the shortest-duration long gamma-ray burst (LGRB).

4.9. *GRB 201130A*

The trigger on GRB 201130A reached a depth of 20.5 mag in the first night of observations after covering 75% of the credible region. No optical transient passed all our filtering criteria (Reusch et al. 2020b).

4.10. *GRB 210510A*

We triggered optical observations on GRB 210510A (trigger 642367205) roughly 10 hrs after the burst. The second night of observations helped with vetting candidates based on their photometric evolution, at least a 0.3 mag/day decay rate is expected for afterglows and KNe. The only candidate that passed our filtering criteria was ZTF21abaytuk (Anand et al. 2021), however its Keck LRIS spectrum showed Mg II, CIII, and OIII absorption features at redshift of 0.89 (see Table 10 and Fig. 5).

4.11. *GRB 210529B*

After two nights of observations covering $\sim$85% of the localization region of GRB 210529B (trigger 644025222), only seven candidates passed our filtering criteria (Ahumada et al. 2021). We reached an average 5σ limit of 22.2 mag in the r-band and in order to determine whether this transients were the optical counterpart, we used the Gemini Multi-object Spectrograph (GMOS) North (G2021A-Q-102, P.I. Ahumada), the Growth India telescope and Wafer-Scale Imager for Prime (WASP) mounted at the P200 telescope. None of the transients showed a fast evolution, thus no optical counterpart was associated to this trigger (see Table 11).

5. ZTF UPPER LIMITS

It is possible to compare the search sensitivity, both in terms of depth and timescale, to the expected afterglow and kilonova light-curves. In left panel of Figure 6, the median limits for ZTF observations are shown with respect to known *Swift* SGRB afterglows with measured redshift from Fong et al. (2015). The yellow light-curve corresponds to GW170817 (Abbott et al. 2017c) and the red line is the same GW170817 light-curve scaled to a distance of 200 Mpc. Along with GW170817, we show a collection of KN light-curves from Bulla (2019) scaled to 250 Mpc. The regions of the light-curve space explored by each ZTF trigger are represented as grey rectangles and the more opaque region corresponds to their intersection. Even though ZTF has the ability to detect a GW170817-like event and most of the Bulla (2019) KN lightcurves, most of the SGRB afterglows observed in the past are below the median sensitivity of the telescope. On the other hand, the counterpart of the GRB 200826A is detected in six of our searches, even though is on the less energetic part of the LGRB distribution. When scaled to 200 Mpc, the GW170817 light-curve overlaps the region of five of our searches, suggesting that the combination of depth and rapid coverage of the regions could allow us to detect an GW170817-like event. The searches that do not overlap with the scaled

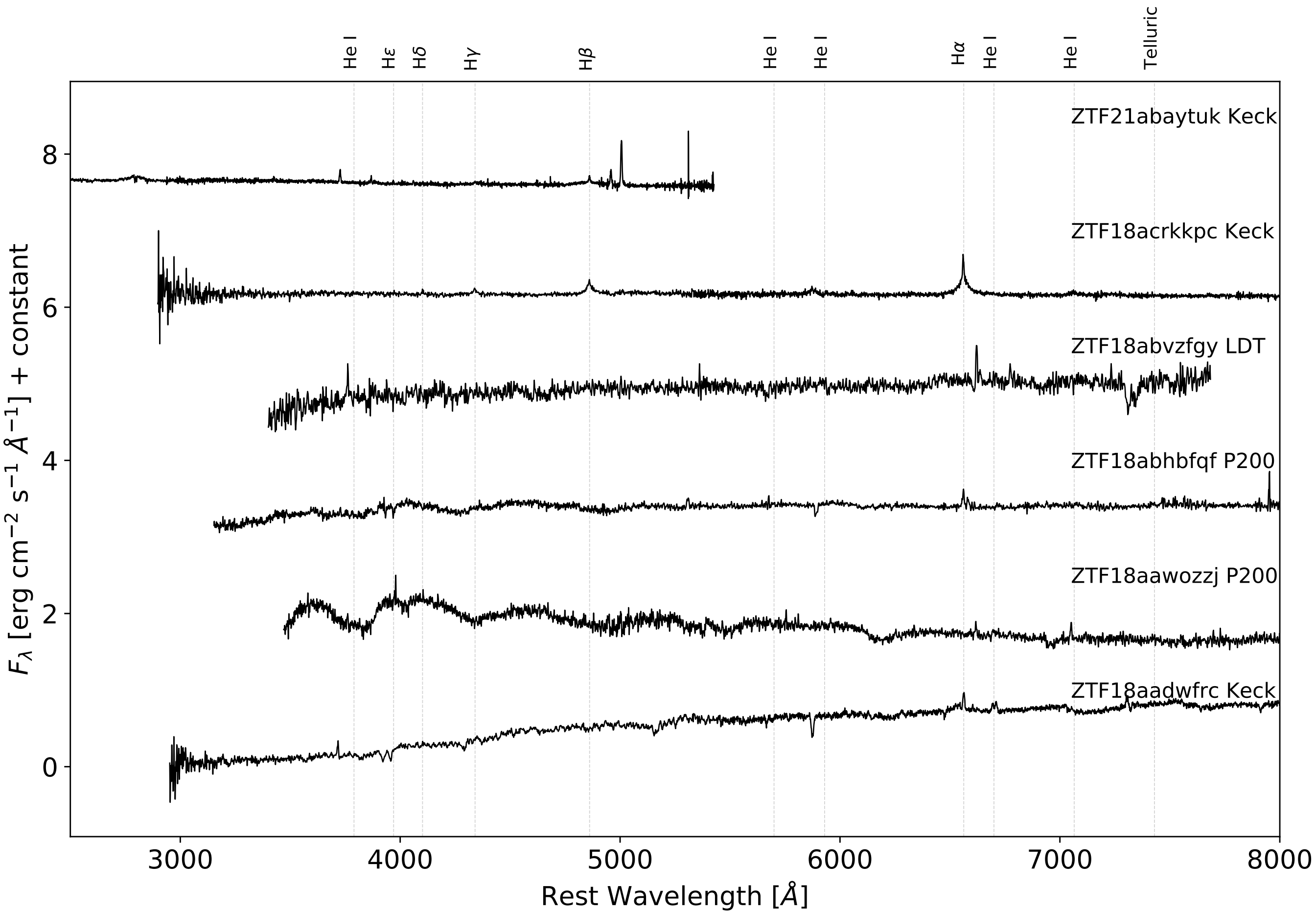

Figure 5. The spectra of some representative candidates. The spectrum of transient ZTF18aadwfrc was taken with the LRIS at the Keck Observatory and was classified as a SN Ia-02cx at $z = 0.04$. Similarly, the spectrum of ZTF18acrkkpc and ZTF21abaytuk come from Keck as well, and were classified as a SN II at $z = 0.061$ and as an AGN at $z = 0.89$ respectively. We used the DBSP at P200 to aqcuire spectra of ZTF18aawozzj and ZTF18abhbfqf, two SN Ia-91T at redshift $z = 0.095$ and $z= 0.11$ respectively. Lastly, the spectrum of ZTF18abvzfgy was obtained with the DeVeny Spectrograph at the LDT, and using `dash`, we classified it as a SN Ic-BL at $z = 0.04$. For reference, we show the Hydrogen, Helium, and some telluric lines as vertical lines.

GW170817 have either fainter median magnitude upper limits (< 20 mag) or late starting times (> 1 day).

We used the redshift of the SGRBs optical counterparts to determine their absolute magnitude, which is plotted in the right panel in Figure 6, along with GRB 200826A and GW170817. In order to compare with the ZTF searches and constrain the observations, the median ZTF limits were scaled to a fiducial distance of 200 Mpc, the LIGO/Virgo detection horizon (Abbott et al. 2018). The distance of distance of 200 Mpc is coincidentally approximately the furthest distance as to which ZTF can detect an GW170817-like event based on the median limiting magnitudes of this experiment. Moreover, the ZTF region covers most of the KNe models (Bulla (2019); blue shaded region) scaled at 200 Mpc. In contrast to the left panel in Figure 6, most of the SGRB optical afterglows fall in the region explored by ZTF. Therefore, if any similar events happened within 200 Mpc, the current ZTF ToO depth plus a rapid trigger of the observations should suffice to ensure coverage in the light-curve space. Previous studies (Dichiara et al. 2020) have come to the conclusion that the low rate of local SGRB is the responsible of the lack of detection GW170817-like transients.

6. EFFICIENCY AND JOINT PROBABILITY OF NON-DETECTION

In order to determine the efficiency of our searches and calculate the likelihood of detecting an SGRB afterglow in one of our ToO triggers, for each GRB, we injected afterglow-like transients in the GRB maps and derived efficiencies using the ZTF observing logs. This approach

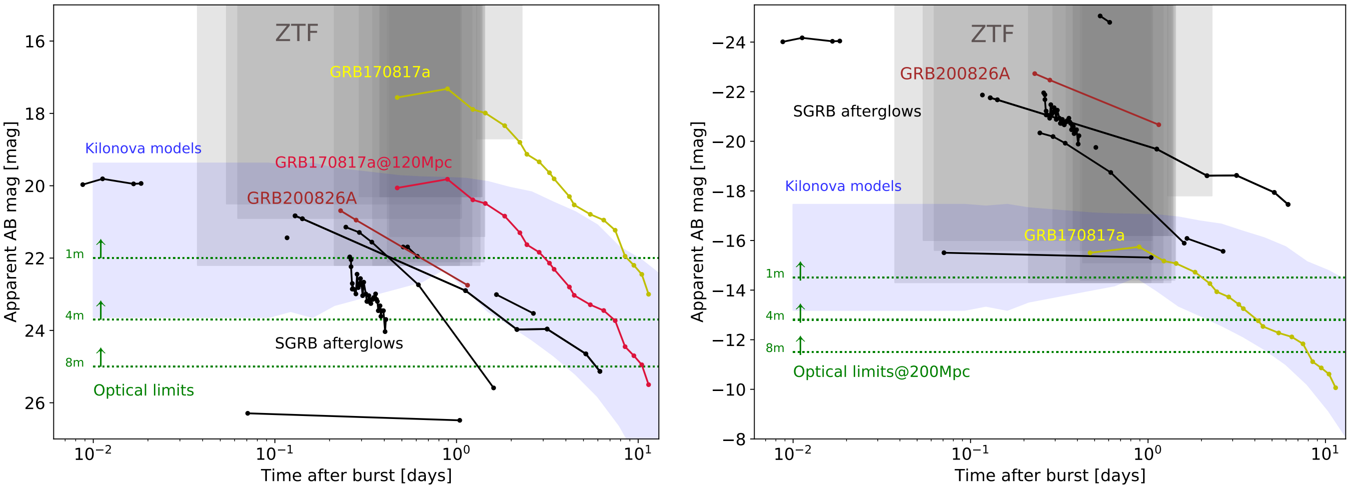

Figure 6. *(left)* The light-curves (black) of the optical counterparts of SGRBs with known redshift listed in Fong et al. (2015). The yellow light-curve is the GW170817 light-curve and the red line is the GW170817 light-curve scaled to a distance of 200 Mpc. Each of the ZTF search windows occupies a grey region, limited by the median limiting magnitude and the time window in which the search took place. The brown light-curve is the afterglow of GRB 200826A Ahumada et al. (2021) and the blue shaded region represents the region that the Bulla (2019) KN models occupy when scaled to 250 Mpc. The green-dotted lines represent the typical optical limits of imagers mounted at different telescopes, while the size of the telescope is annotated as a label in the plot. *(right)* The absolute magnitude of the same data plotted in the left panel. We compare their absolute magnitudes to the ZTF magnitude limits, scaled to a fiducial distance of 200 Mpc. Similarly, the green-dotted lines show the optical limits of different facilities, ranging in size, at 200 Mpc.

already takes into consideration weather and other unexpected problems with the survey. In this section we describe the computational tools used in this endeavor and the results derived from these simulations.

One of the driving features of an afterglow model is its isotropic-equivalent energy, E_{iso}, as it sets the luminosity of the burst and hence its magnitude. The information provided by the *Fermi*-GBM γ-ray detections do not give insights on the distance at which the event happened or the energies associated with the SGRBs. For this reason, we assume that our population of SGRBs follows the isotropic energy (E_{iso}) - rest-frame peak energy (E_z, p) relationship (see Eq. 1), postulated in Equation 2 of Tsutsui et al. 2013. This relationship requires the peak energies of the bursts, E_p, which can be obtained by fitting a Band model (Band et al. 1993) to the γ-ray emission over the duration of the burst. The results of this modelling are usually listed on the public GBM catalog (von Kienlin et al. 2020) and online[9]. The compilation of E_p for our SGRBs sample is listed in Table 1.

$$E_{iso} = 10^{52.42\pm-0.15}\, erg \left(\frac{E_{z,p}}{774.5\ keV}\right)^{1.58\pm0.28} \tag{1}$$

The energies that result from this transformation are usually larger than the energies derived for previous SGRB afterglows. We also use the average kinetic isotropic energy, $E_{K,iso}$, presented in Fong et al. (2015) as a representative value for E_{iso}. Particularly, we assume $E_{K,iso} \sim E_{iso} = 2.9 \times 10^{51}$ ergs.

We have used the python module `afterglowpy` (Ryan et al. 2020) to generate afterglow light-curves templates. Due to the nature of the relativistic jet, we constrained the viewing angle to $\theta < 20°$. We assume a circumburst density of 5.2×10^{3}, we chose a Gaussian jet, and we fixed other `afterglowpy` parameters to standard values: the electron energy distribution index $p = 2.43$, as well as $\epsilon_E = 0.1$ and $\epsilon_B = 0.01$. For the E_{iso}, we used the relation in Eq. 1 and the mean $E_{K,iso}$ mentioned in the paragraph above. Additionally for E_{iso} as a function of $E_{z,p}$, we took the gamma-ray $E_{z,p} = E_p(1+z)$, with the redshift varying for each simulated source.

We injected the afterglow light-curves created with `afterglowpy` into the GBM skymaps using `simsurvey` (Feindt et al. 2019). This tool is designed to inject transients on the sky and measure the recovery power of a given observing strategy. For any given transient, `simsurvey` can derive the magnitude of the event and whether or not it was detected, based on the observing strategy and observational limits of any given ZTF field. We randomly distributed the afterglows previously gen-

---

[9] https://heasarc.gsfc.nasa.gov/W3Browse/fermi/fermigbrst.html

erated on the 90% credible level of each GRB skymap and calculated the efficiency as the ratio of sources detected *twice* versus the number of generated sources. We require two detections as our ToO strategy relies on at least two data points.

The efficiencies vary depending on a few factors. The total coverage and the limiting magnitude of the observations limit the maximum efficiency, which then decays depending on the associated E_{iso}. For larger energies, the decay is smoother. In the top panel of Fig. 7, we show the efficiencies for the 10 GRBs that had no counterpart. We exclude GRB 200826A as the energies used to model the afterglow follow the SGRB energy distribution, while GRB 200826A was proven to be part of the LGRB population. The energies derived from the Tsutsui et al. (2013) relationship are larger than the mean $E_{K,iso}$ derived from Fong et al. (2015). This increases the efficiencies at larger redshifts, as the transients are intrinsically more energetic.

For both of the energies used, we calculate the joint probability of non-detection by taking the product of the SGRB ToO efficiencies as a function of redshift. Similar to the analysis in Kasliwal et al. (2020), we define

$$(1 - CL) = \prod_{i=0}^{N}(1 - p_i) \tag{2}$$

with CL as the credible level and p_i the efficiency of the ith burst as a function of redshift. We show in the bottom panel of Fig. 7 the result for the afterglows with energies following Tsutsui et al. (2013) (blue) and Fong et al. (2015) (yellow). The lower energies associated with Fong et al. (2015) afterglows only allow us to probe the space up to z = 0.2, considering a $CL = 0.9$, while SGRBs with energies following the $E_{iso} - E_{z,p}$ relationship can be probed as far as z = 0.35. To look into the prospects of the SGRB ToO campaign, we model a scenario with 30 additional follow-up campaigns, each with a median efficiency based on the results presented here. These results are shown as dashed lines in Fig. 7, and show that for $E_{iso} \sim E_{K,iso}$, the improvement after thirty TOOs can only expand our searches (i.e. $CL = 0.9$) up to z = 0.25, while if the GRBs follow the $E_{iso} - E_{z,p}$ relationship, our horizon expands to z = 0.9. Compared to the redshift distribution of SGRB afterglows, our searches show a compelling case.

7. PROPOSED FOLLOW-UP STRATEGY

The current ToO strategy aims for two consecutive exposures in two different filters, prioritizing the color of the source as the main avenue to discriminate between sources. This helps confirming the nature of the transient as an extragalactic source. In some cases, it can lead to a problems as the source might not be detected at higher wavelengths, due to either the extinction along the line of sight or its intrinsically fainter brightness. If there is no second detection at higher wavelengths, there is the risk of ignoring a potential counterpart as a single detection can be confused as a slow moving object or an artifact. The standard strategy considers a second night of ZTF observations in the same two filters, to measure the magnitude and color evolution. However, a number of sources did not have a second detection in the same filter after the second night, impeding the measurement of the decay rate. For these two reasons, for afterglow searches with ZTF (and possibly other instruments with similar limiting magnitudes), it is more informative to observe the region at least twice in the same filter during the first night. By separating the two same-filter epochs by at least $2\sigma \times 24/\alpha$, where σ is the typical error of the observations and α is the power-law index of the afterglow, we can possibly measure the decay rate of sources, or at least set a lower limit for α. For ZTF, two epochs separated by 6 hours would suffice for afterglows with a typical $\alpha \sim 1$, assuming $\sigma = 0.12$.

This scenario is unlikely to happen often, as it requires that the region is visible during the entire night and that the night is long enough to allow for two visits separated by a number of hours. In any case, the standard ToO strategy for the second night of observation (two visits in two different filters) should help determine the color and magnitude evolution.

For the third day of follow-up, there will be two kinds of candidates: (a) confirmed fast fading transients, and (b) transients with unconstrained evolution, that likely only have data for the first night. For (a) it is important to get spectra as soon as possible before the transients fade below the spectroscopic limits. Ideally, observations in other wavelengths should be triggered to cement the classification and begin the characterization of the transient. For candidates in situation (b), the fast evolution of the transients requires the use of larger facilities. From our experience, this is feasible as only a handful of candidates will fall in this category. In both cases, (a) and (b), photometric follow-up using facilities different than ZTF are needed, as any afterglow detected by ZTF will not be detectable three days after the burst. In Fig. 8 we show the magnitude distribution of all the transients that `simsurvey` detected, independent of redshift, as a function of the how many days passed after the burst. This figure illustrates the need for other telescopes to monitor the evolution of the transient, as for example, only ∼30% of the transients that we can detect with ZTF will be brighter than $r > 22$ mag. Additionally, Fig. 8 shows that spectroscopy of the sources becomes harder after day 2, as only 20% of the detected transients will be brighter than $r = 21.5$ mag.

Since spectroscopic data will be challenging to acquire for faint sources, the panchromatic follow-up, from radio to x-rays, will help to confirm the classification of the transient.

8. CONCLUSIONS

During a period of ∼2 years, a systematic, extended and deep search for the optical counterpart to *Fermi*-GBM SGRBs has been performed employing the Zwicky Transient Facility. The ZTF observations of the 11 events followed-up are listed in Table 3 and no optical counterpart has yet been associated to a compact binary coalescence. However, our ToO strategy led to the discovery of the optical counterpart to GRB 200826A, which was ultimately revealed as the shortest-duration LGRB found to date.

This experiment complements previous studies (Singer et al. 2013, 2015; Coughlin et al. 2019a; Ahumada et al. 2021), and demonstrates the feasibility of studying the large sky areas derived from *Fermi* GBM by exploiting the wide field of view of ZTF. The average coverage was $\sim$ 60% of the localization regions, corresponding to $\sim$ 950 deg^2. The average amount of alerts in the targeted regions of the sky was over 20000, and we were able to reduce this figure to no more than 20 candidates per trigger. Thanks to the high cadence of ZTF we were able to achieve a median reduction in alerts of 0.04%. The effectiveness of the filtering criteria is comparable with the median reduction reached in Singer et al. (2015), even when the areas covered are almost orders of magnitude larger. In fact, the iPTF search for the optical counterparts to the long gamma-ray burst GRB 130702A covered 71 degrees squared and yielded 43 candidates (Singer et al. 2013).

This campaign has utilized ZTF capabilities to rapidly follow-up SGRB trigger, which has allowed us to explore the magnitude space and set constraints to SGRBs events. The average upper limit for ZTF 300s exposures is $r \sim 20.8$ which has allowed us to look for SGRB afterglows and GW170817-like KNe. From Figure 8, it can be seen that future follow-ups would benefit both from a more rapid response and longer exposures.

By using computational tools like `afterglowpy` and `simsurvey`, we have quantified the efficiency of our ToO triggers. The ZTF efficiency drops quickly as the transient is located at further distances, and the magnitude limits only allow for detections up to z = 0.4, for energies following the Tsutsui et al. (2013) relation and z = 0.2 for bursts with energies equal to the mean E_{iso} found by Fong et al. (2015), for a $CL = 0.9$. Furthermore, when repeating the experiment 30 times while assuming a median efficiency p_{med}, the horizons of our searches increase to z = 0.25 and 0.9 respectively.

Additionally, our simulations show that ZTF is no longer effective at following-up afterglows after three days following the burst. The fast fading nature of these transients requires deeper observations, and spectroscopic and panchromatic observations are helpful to reveal the nature of the candidates. Ideally, at least two observations in the same filter should be taken during the first night of observation, as afterglows and KN fade extremely rapidly and they might not be observable 48 hrs after the burst. With this strategy we can hope to find another counterpart.

Based on observations obtained with the Samuel Oschin Telescope 48-inch and the 60-inch Telescope at the Palomar Observatory as part of the Zwicky Transient Facility project. ZTF is supported by the National Science Foundation under Grant No. AST-1440341 and a collaboration including Caltech, IPAC, the Weizmann Institute for Science, the Oskar Klein Center at Stockholm University, the University of Maryland, the University of Washington, Deutsches Elektronen-Synchrotron and Humboldt University, Los Alamos National Laboratories, the TANGO Consortium of Taiwan, the University of Wisconsin at Milwaukee, and Lawrence Berkeley National Laboratories. Operations are conducted by COO, IPAC, and UW. This work was supported by the GROWTH (Global Relay of Observatories Watching Transients Happen) project funded by the National Science Foundation under PIRE Grant No 1545949. GROWTH is a collaborative project among California Institute of Technology (USA), University of Maryland College Park (USA), University of Wisconsin Milwaukee (USA), Texas Tech University (USA), San Diego State University (USA), University of Washington (USA), Los Alamos National Laboratory (USA), Tokyo Institute of Technology (Japan), National Central University (Taiwan), Indian Institute of Astrophysics (India), Indian Institute of Technology Bombay (India), Weizmann Institute of Science (Israel), The Oskar Klein Centre at Stockholm University (Sweden), Humboldt University (Germany), Liverpool John Moores University (UK) and University of Sydney (Australia). TA thanks the LSSTC Data Science Fellowship Program, which is funded by LSSTC, NSF Cybertraining Grant #1829740, the Brinson Foundation, and the Moore Foundation; his participation in the program has benefited this work. SRM and JC acknowledge support from the NSF grant NSF PHY #1912649. We are grateful for computational resources provided by the Leonard

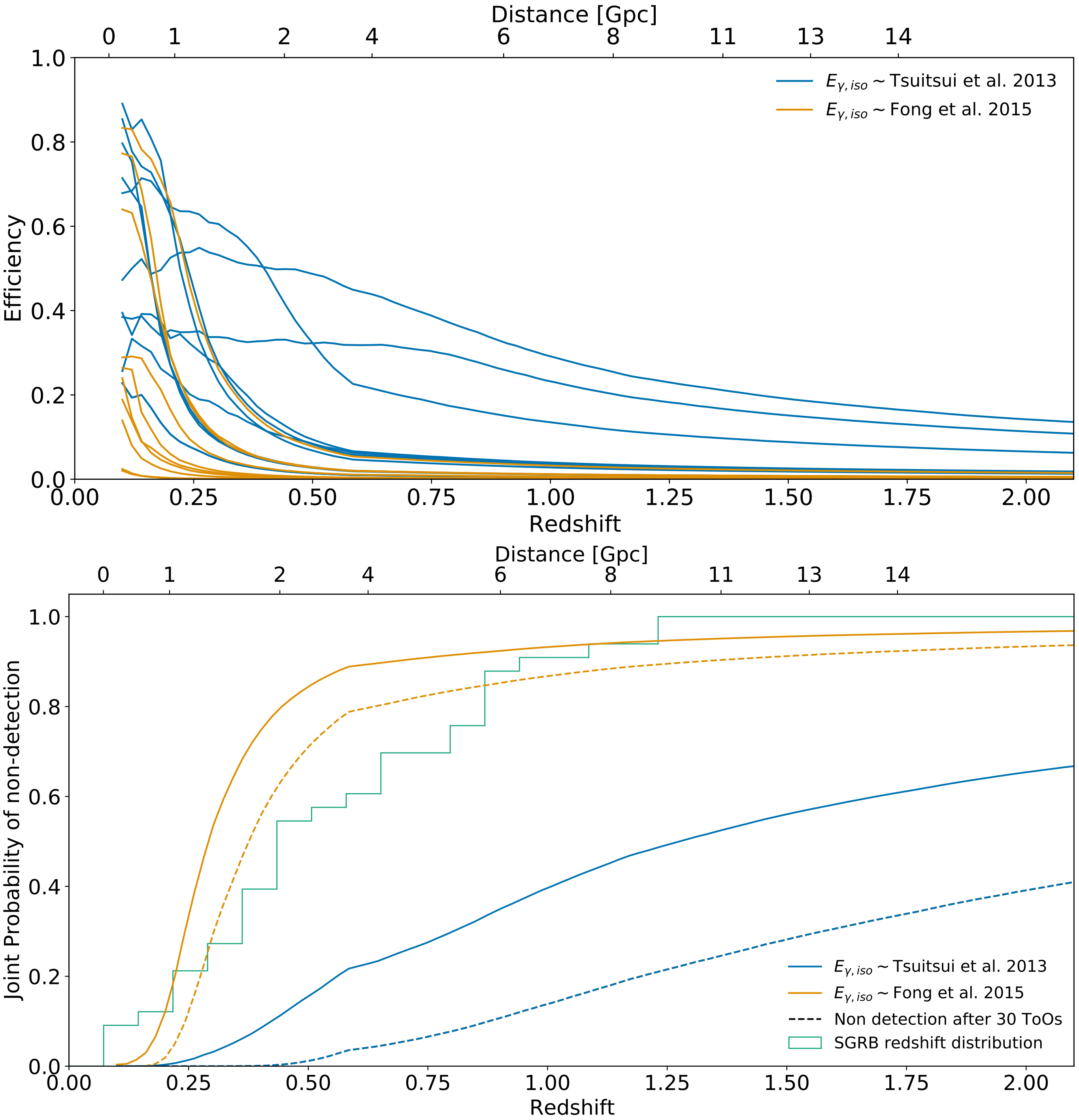

Figure 7. (top) The individual efficiency for each SGRB trigger. The blue curves are based on the E_{iso} derived from the Band model E_p and Eq. 1, while the yellow curves are the effiencies assuming all GRBs have the same E_{iso} as the mean $E_{K,iso}$ from Fong et al. (2015). (bottom) The solid lines represent the joint probability of non-detection using the 10 SGRB triggers with no optical counterparts. we adopt the same color coding as in the top plot, meaning blue for the E_{iso} as a function of E_p and yellow for E_{iso} as the mean $E_{K,iso}$ from Fong et al. (2015). The dashed line represent the joint probability of non-detection after 30 TOOs, assuming an efficiency equal to the median efficiency of the TOOs presented. We show the cumulative redshift distribution for SGRBs as a turquoise line.

GRB	Area covered	C.R. covered	Trigger delay time	Exposure time (sequence)	r-band 5σ limit	Objects followed-up
GRB 180523B	2900 deg^2	60%	9.1h	60s(rgr), 90s(rgr)	r > 20.3 mag	14
GRB 180626C	275 deg^2	87%	1.5h	120s(rgr), 240s(grg)	r > 20.9 mag	1
GRB 180715B	254 deg^2	37%	10.3h	180s(rgr), 240s(rg)	r > 21.4 mag	14
GRB 180728B	334 deg^2	76%	31h	180s(rgr), 180s(rgr)	r > 18.7 mag	7
GRB 180913A	546 deg^2	53%	8.3h	180s(grg), 300s(grg)	r > 22.2 mag	12
GRB 181126B	1400 deg^2	66%	1.3h	180s(rr), 300s (r)	r > 20.5 mag	11
GRB 200514B	519 deg^2	49%	0.9h	300s(gr)	r > 22.2 mag	14
GRB 201130A	400 deg^2	75%	7h	300s(grg),300s(gr)	r > 20.3 mag	0
GRB 210510A	1105 deg^2	84%	10h	180(gr),240(r)	r > 22.1 mag	1
GRB 210529B	686 deg^2	85%	5.1h	180s(gr),180s(gr)	r > 22.2 mag	14

Table 3. Summary of the ZTF ToO triggers. We list the area covered with ZTF, as well as the corresponding credible region (C.R.) of the GBM map. The trigger delay time represents the amount of time between the burst and the start of ZTF observations. For each trigger, we list the exposure time for night 1 and nigth 2, along with the filter sequence in parenthesis. The last two columns show the median r-band 5σ limit and the number of objects followed-up with other facilities.

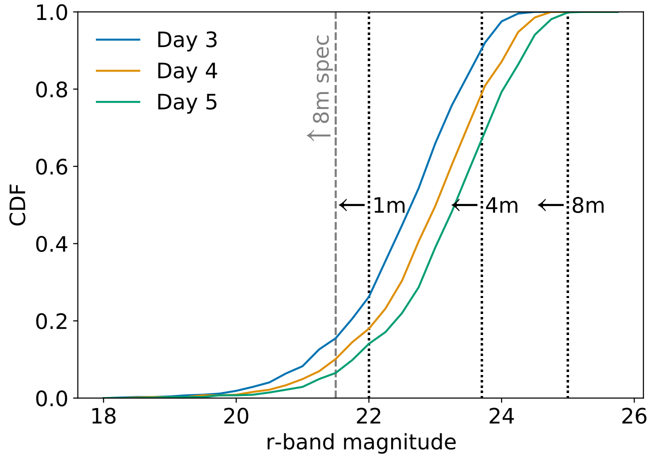

Figure 8. The magnitude cumulative distribution of the sources detected using `simsurvey` as a function of the days after the burst. This distribution contains all the sources detected up to z=2. The photometric and spectroscopic limits of different facilities are shown as dotted vertical lines.

E Parker Center for Gravitation, Cosmology and Astrophysics at the University of Wisconsin-Milwaukee. MMK acknowledges generous support from the David and Lucille Packard Foundation. M.W.C. acknowledges support from the National Science Foundation with grant Nos. PHY-2010970 and OAC-2117997. S.A. acknowledges support from the GROWTH PIRE Grant No 1545949. A.S.C acknowledges support from the G.R.E.A.T research environment, funded by *Vetenskapsrådet*, the Swedish Research Council, project number 2016-06012. M.B. acknowledges support from the Swedish Research Council (Reg. no. 2020-03330). We thank the reviewer whose comments and suggestions helped improve and clarify this manuscript.

This work was supported by the GROWTH (Global Relay of Observatories Watching Transients Happen) project funded by the National Science Foundation under PIRE grant No. 1545949. GROWTH is a collaborative project among California Institute of Technology (USA), University of Maryland College Park (USA), University of Wisconsin Milwaukee (USA), Texas Tech University (USA), San Diego State University (USA), University of Washington (USA), Los Alamos National Laboratory (USA), Tokyo Institute of Technology (Japan), National Central University (Taiwan), Indian Institute of Astrophysics (India), Indian Institute of Technology Bombay (India), Weizmann Institute of Science (Israel), The Oskar Klein Centre at Stockholm University (Sweden), Humboldt University (Germany), Liverpool John Moores University (UK) and University of Sydney (Australia). Based on observations obtained with the Samuel Oschin Telescope 48-inch and the 60-inch Telescope at the Palomar Observatory as part of the Zwicky Transient Facility project. ZTF is supported by the National Science Foundation under grant No. AST-1440341 and a collaboration including Caltech, IPAC, the Weizmann Institute for Science, the Oskar Klein Center at Stockholm University, the University of Maryland, the University of Washington (UW), Deutsches Elektronen-Synchrotron and Humboldt University, Los Alamos National Laboratories, the TANGO Consortium of Taiwan, the University of Wisconsin at Milwaukee and Lawrence Berkeley National Laboratories. Operations are conducted by Caltech Optical Observatories, IPAC and UW. The material is based on work supported by NASA under award No. 80GSFC17M0002. Based on observations obtained at the international Gemini Observatory, a program of NSF's NOIRLab, which is managed by the Association of Universities for Research in Astronomy (AURA) under a cooperative agreement with the National Science Foundation on behalf of the Gemini Observatory partnership: the National Science Foundation (United States), National Research Council (Canada), Agencia Nacional de Investigación y Desarrollo (Chile), Ministerio de Ciencia, Tecnología e Innovación (Argentina), Ministério da Ciência, Tecnologia, Inovações e Comunicações (Brazil), and Korea Astronomy and Space Science Institute (Republic of Korea). The observations were obtained as part of Gemini Director's Discretionary Program GN-2021A-Q-102. The Gemini data was processed using DRAGONS (Data Reduction for Astronomy from Gemini Observatory North and South). This work was enabled by observations made from the Gemini North telescope, located within the Maunakea Science Reserve and adjacent to the summit of Maunakea. We are grateful for the privilege of observing the Universe from a place that is unique in both its astronomical quality and its cultural significance. The ZTF forced-photometry service was funded under the Heising-Simons Foundation grant No. 12540303 (PI: Graham). These results also made use of Lowell Observatory's Lowell Discovery Telescope (LDT), formerly the Discovery Channel Telescope (LDT). Lowell operates the LDT in partnership with Boston University, Northern Arizona University, the University of Maryland and the University of Toledo. Partial support of the LDT was provided by Discovery Communications. LMI was built by Lowell Observatory using funds from the National Science Foundation (AST-1005313). M.W.C. acknowledges support from the National Science Foundation with grant No. PHY-2010970. S.A. gratefully acknowledges support from the GROWTH PIRE grant (1545949). E.C.K. acknowledges support from the G.R.E.A.T research environment and the Wenner-Gren Foundations. T.A. and H.K. are LSSTC Data Science Fellows and thank the LSSTC Data Science Fellowship Program, which is funded by LSSTC, NSF Cybertraining grant No. 1829740, the Brinson Foundation and the Moore Foundation; their participation in the program has benefited this work.

Software: `ipython` (Pérez & Granger 2007), `jupyter` (Kluyver et al. 2016), `matplotlib` (Hunter 2007), `python` (Van Rossum & Drake 2009), `NumPy` (Harris et al. 2020), `scikit-learn` (Pedregosa et al. 2011), `scipy` (Virtanen et al. 2020)

Facilities: LIGO, ZTF/PO:1.2m

REFERENCES

Abbott et al. 2017a, Phys. Rev. Lett., 119, 161101. https://link.aps.org/doi/10.1103/PhysRevLett.119.161101

—. 2017b, The Astrophysical Journal Letters, 848, L13. http://stacks.iop.org/2041-8205/848/i=2/a=L13

—. 2017c, Phys. Rev. Lett., 118, 221101

—. 2018, Living Reviews in Relativity, 21, 3. https://doi.org/10.1007/s41114-018-0012-9

Ahumada, R., Allende Prieto, C., Almeida, A., et al. 2020a, ApJS, 249, 3

Ahumada, T., Kumar, H., Fremling, C., et al. 2020b, GRB Coordinates Network, 29029, 1

Ahumada, T., Coughlin, M. W., Cenko, S. B., et al. 2018, GRB Coordinates Network, 23515, 1

Ahumada, T., Anand, S., Andreoni, I., et al. 2020, GRB Coordinates Network, 27737, 1

Ahumada, T., Anand, S., Stein, R., et al. 2020, GRB Coordinates Network, 28295, 1

Ahumada, T., Singer, L. P., Anand, S., et al. 2021, Nature Astronomy, 5, 917

Ahumada, T., Anand, S., Kumar, H., et al. 2021, GRB Coordinates Network, 30109, 1

Almualla, M., Coughlin, M. W., Anand, S., et al. 2020, MNRAS, 495, 4366

Amati, L. 2021, Nature Astronomy, 5, 877

Anand, S., Coughlin, M. W., Kasliwal, M. M., et al. 2020, Nature Astronomy, arXiv:2009.07210

Anand, S., Andreoni, I., Ahumada, T., et al. 2021, GRB Coordinates Network, 30005, 1

Andreoni, I., Goldstein, D. A., Anand, S., et al. 2019, ApJL, 881, L16

Andreoni, I., Goldstein, D. A., Kasliwal, M. M., et al. 2020, ApJ, 890, 131

Andreoni, I., Kool, E. C., Carracedo, A. S., et al. 2020, The Astrophysical Journal, 904, 155

Andreoni, I., Coughlin, M. W., Kool, E. C., et al. 2021, arXiv preprint arXiv:2104.06352

Arcavi, I., Hosseinzadeh, G., Howell, D. A., et al. 2017, Nature, 551, 64

Band, D., Matteson, J., Ford, L., et al. 1993, The Astrophysical Journal, 413, 281

Bellm, E. C., & Sesar, B. 2016, pyraf-dbsp: Reduction pipeline for the Palomar Double Beam Spectrograph, , , ascl:1602.002

Bellm, E. C., Kulkarni, S. R., Graham, M. J., et al. 2018, Publications of the Astronomical Society of the Pacific, 131, 018002

Berger, E., Price, P. A., Cenko, S. B., et al. 2005, Nature, 438, 988

Bertin, E., & Arnouts, S. 1996, Astron. Astrophys. Suppl. Ser., 117, 393. https://doi.org/10.1051/aas:1996164

Blagorodnova, N., Neill, J. D., Walters, R., et al. 2018, PASP, 130, 035003

Blondin, S., & Tonry, J. L. 2007, ApJ, 666, 1024

Bloom, J. S., Kulkarni, S. R., Djorgovski, S. G., et al. 1999, Nature, 401, 453–456. http://dx.doi.org/10.1038/46744

Bromberg, O., Nakar, E., Piran, T., & Sari, R. 2013, The Astrophysical Journal, 764, 179. http://stacks.iop.org/0004-637X/764/i=2/a=179

Brown, T. M., Baliber, N., Bianco, F. B., et al. 2013, Publications of the Astronomical Society of the Pacific, 125, 1031. https://doi.org/10.1086%2F673168

Bulla, M. 2019, MNRAS, 489, 5037

Burns, E., Svinkin, D., Hurley, K., et al. 2021, The Astrophysical Journal Letters, 907, L28

Cannizzo, J. K., & Gehrels, N. 2009, The Astrophysical Journal, 700, 1047. http://stacks.iop.org/0004-637X/700/i=2/a=1047

Cano, Z., Wang, S.-Q., Dai, Z.-G., & Wu, X.-F. 2017, Advances in Astronomy, 2017

Cenko, S. B., Coughlin, M. W., Ghosh, S., et al. 2018, GRB Coordinates Network, 22969, 1

Chambers, K. C., Magnier, E. A., Metcalfe, N., et al. 2016, arXiv e-prints, arXiv:1612.05560

Chatterjee, D., Nugent, P. E., Brady, P. R., et al. 2019, The Astrophysical Journal, 881, 128

Chornock, R., Berger, E., Kasen, D., et al. 2017, ApJL, 848, L19

Chornock et al. 2017, The Astrophysical Journal Letters, 848, L19. http://stacks.iop.org/2041-8205/848/i=2/a=L19

Côté, B., Fryer, C. L., Belczynski, K., et al. 2018, The Astrophysical Journal, 855, 99

Coughlin, M. W., Ahumada, T., Cenko, B., et al. 2018a, GRB Coordinates Network, 23379, 1

Coughlin, M. W., Singer, L. P., Cenko, S. B., et al. 2018b, GRB Coordinates Network, 22739, 1

Coughlin, M. W., Tao, D., Chan, M. L., et al. 2018, Monthly Notices of the Royal Astronomical Society, 478, 692. http://dx.doi.org/10.1093/mnras/sty1066

Coughlin, M. W., Singer, L. P., Ahumada, T., et al. 2018a, GRB Coordinates Network, 22871, 1

Coughlin, M. W., Cenko, S. B., Ahumada, T., et al. 2018b, GRB Coordinates Network, 23324, 1

Coughlin, M. W., Ahumada, T., Cenko, S. B., et al. 2019a, PASP, 131, 048001

Coughlin, M. W., Ahumada, T., Anand, S., et al. 2019b, ApJL, 885, L19

Coughlin, M. W., Antier, S., Corre, D., et al. 2019a, Mon. Not. R. Astron. Soc., http://oup.prod.sis.lan/mnras/advance-article-pdf/doi/10.1093/mnras/stz2485/29808472/stz2485.pdf, stz2485. https://doi.org/10.1093/mnras/stz2485

Coughlin, M. W., Dekany, R. G., Duev, D. A., et al. 2019b, Monthly Notices of the Royal Astronomical Society, 485, 1412–1419. http://dx.doi.org/10.1093/mnras/stz497

Coulter, D. A., Foley, R. J., Kilpatrick, C. D., et al. 2017, Science, 358, 1556

Cowperthwaite, P. S., Berger, E., Villar, V. A., et al. 2017a, ApJL, 848, L17

—. 2017b, ApJL, 848, L17

Cutri, R. M., Wright, E. L., Conrow, T., et al. 2013, Explanatory Supplement to the AllWISE Data Release Products, Explanatory Supplement to the AllWISE Data Release Products, ,

D'Avanzo, P. 2015, Journal of High Energy Astrophysics, 7, 73

De, K., Hankins, M. J., Kasliwal, M. M., et al. 2020, PASP, 132, 025001

Dichiara, S., Troja, E., O'Connor, B., et al. 2020, Monthly Notices of the Royal Astronomical Society, 492, 5011

Djorgovski, S. G., Drake, A. J., Mahabal, A. A., et al. 2011, arXiv e-prints, arXiv:1102.5004

Djupvik, A. A., & Andersen, J. 2010, in Highlights of Spanish astrophysics V (Springer), 211–218

Drout, M. R., Piro, A. L., Shappee, B. J., et al. 2017, Science, 358, 1570

Duev, D. A., Mahabal, A., Masci, F. J., et al. 2019, Monthly Notices of the Royal Astronomical Society, 489, 3582

Duffell, P. C., & MacFadyen, A. I. 2015, The Astrophysical Journal, 806, 205. http://stacks.iop.org/0004-637X/806/i=2/a=205

Evans, P. A., Cenko, S. B., Kennea, J. A., et al. 2017, Science, 358, 1565

Feindt, U., Nordin, J., Rigault, M., et al. 2019, Journal of Cosmology and Astroparticle Physics, 2019, 005

Flesch, E. W. 2019, arXiv e-prints, arXiv:1912.05614

Fong, W., Berger, E., Margutti, R., & Zauderer, B. A. 2015, The Astrophysical Journal, 815, 102. http://stacks.iop.org/0004-637X/815/i=2/a=102

Fong, W., Margutti, R., Chornock, R., et al. 2016, ApJ, 833, 151

Fong, W., Laskar, T., Rastinejad, J., et al. 2021, ApJ, 906, 127

Fremling, C., Sollerman, J., Taddia, F., et al. 2016, A&A, 593, A68

Gal-Yam, A., Fox, D., & MacFayden, A. 2006, Nature, 1053. https://doi.org/10.1038/nature05373

Goldstein, A., Veres, P., Burns, E., et al. 2017, The Astrophysical Journal Letters, 848, L14

Goldstein, D. A., Andreoni, I., Nugent, P. E., et al. 2019, ApJL, 881, L7

Graham, M. J., Kulkarni, S., Bellm, E. C., et al. 2019a, Publications of the Astronomical Society of the Pacific, 131, 078001

—. 2019b, arXiv preprint arXiv:1902.01945

Hamburg, R., Veres, P., & Meegan, C. 2018, GCN, 23057, 1

Harris, C. R., Millman, K. J., van der Walt, S. J., et al. 2020, Nature, 585, 357–362

Hosseinzadeh, G., Cowperthwaite, P. S., Gomez, S., et al. 2019, ApJL, 880, L4

Hunter, J. D. 2007, Computing in Science Engineering, 9, 90

Kasen, D., Metzger, B., Barnes, J., Quataert, E., & Ramirez-Ruiz, E. 2017, Nature, 551, 80 EP . http://dx.doi.org/10.1038/nature24453

Kasen, D., Metzger, B., Barnes, J., Quataert, E., & Ramirez-Ruiz, E. 2017, Nature, 551, 80

Kasliwal, M. M., Nakar, E., Singer, L. P., et al. 2017, Science, 358, 1559. http://science.sciencemag.org/content/358/6370/1559

Kasliwal, M. M., Nakar, E., Singer, L. P., et al. 2017, Science, 358, 1559

Kasliwal, M. M., Anand, S., Ahumada, T., et al. 2020, arXiv preprint arXiv:2006.11306

Kasliwal et al. 2018, Submitted to PASP

Kilpatrick et al. 2017, Science, 358, 1583. http://science.sciencemag.org/content/358/6370/1583

Klebesadel, R. W., Strong, I. B., & Olson, R. A. 1973, The Astrophysical Journal Letters, 182, L85

Kluyver, T., Ragan-Kelley, B., Pérez, F., et al. 2016, in Positioning and Power in Academic Publishing: Players, Agents and Agendas, ed. F. Loizides & B. Scmidt (Netherlands: IOS Press), 87–90. https://eprints.soton.ac.uk/403913/

Kotani, T., Kawai, N., Yanagisawa, K., et al. 2007, arXiv preprint astro-ph/0702708

Kouveliotou, C., Meegan, C. A., Fishman, G. J., et al. 1993, The Astrophysical Journal, 413, L101

Kumar, P., & Granot, J. 2003, The Astrophysical Journal, 591, 1075

Labrie, K., Anderson, K., Cárdenes, R., Simpson, C., & Turner, J. E. H. 2019, in Astronomical Society of the Pacific Conference Series, Vol. 523, Astronomical Data Analysis Software and Systems XXVII, ed. P. J. Teuben, M. W. Pound, B. A. Thomas, & E. M. Warner, 321

Lattimer, J. M., & Schramm, D. N. 1974, ApJL, 192, L145

Law et al. 2009, Publications of the Astronomical Society of the Pacific, 121, 1395. http://stacks.iop.org/1538-3873/121/i=886/a=1395

Lazzati, D., López-Cámara, D., Cantiello, M., et al. 2017, The Astrophysical Journal Letters, 848, L6. http://stacks.iop.org/2041-8205/848/i=1/a=L6

Li, L.-X., & Paczynski, B. 1998, The Astrophysical Journal Letters, 507, L59. http://stacks.iop.org/1538-4357/507/i=1/a=L59

Lipunov, V., Kornilov, V., Krylov, A., et al. 2005, Astrophysics, 48, 389

Lipunov et al. 2017, The Astrophysical Journal Letters, 850, L1. http://stacks.iop.org/2041-8205/850/i=1/a=L1

MacFarlane, M. J., & Dunham, E. W. 2004, Optical design of the Discovery Channel Telescope, , , doi:10.1117/12.550633. https://doi.org/10.1117/12.550633

Mahabal, A., Rebbapragada, U., Walters, R., et al. 2019, Publications of the Astronomical Society of the Pacific, 131, 038002. https://doi.org/10.1088%2F1538-3873%2Faaf3fa

Masci, F. J., Laher, R. R., Rusholme, B., et al. 2019, PASP, 131, 018003

McCully, C., Hiramatsu, D., Howell, D. A., et al. 2017, ApJL, 848, L32

Meegan, C., Lichti, G., Bhat, P. N., et al. 2009, The Astrophysical Journal, 702, 791. https://doi.org/10.1088%2F0004-637x%2F702%2F1%2F791

Mészáros, P., & Rees, M. J. 1998, The Astrophysical Journal Letters, 502, L105. http://stacks.iop.org/1538-4357/502/i=2/a=L105

Metzger, B. D., Giannios, D., Thompson, T. A., Bucciantini, N., & Quataert, E. 2011, Monthly Notices of the Royal Astronomical Society, 413, 2031. http://dx.doi.org/10.1111/j.1365-2966.2011.18280.x

Metzger, B. D., Martínez-Pinedo, G., Darbha, S., et al. 2010, Monthly Notices of the Royal Astronomical Society, 406, 2650

Metzger, M., Djorgovski, S., Kulkarni, S., et al. 1997, Nature, 387, 878

Mong, Y., Ackley, K., Galloway, D., et al. 2021, Monthly Notices of the Royal Astronomical Society, 507, 5463

Mooley, K. P., Nakar, E., Hotokezaka, K., et al. 2017, Nature, 554, 207 EP . http://dx.doi.org/10.1038/nature25452

Morrissey, P., Conrow, T., Barlow, T. A., et al. 2007, ApJS, 173, 682

Muthukrishna, D., Parkinson, D., & Tucker, B. E. 2019, ApJ, 885, 85

Nagakura, H., Hotokezaka, K., Sekiguchi, Y., Shibata, M., & Ioka, K. 2014, The Astrophysical Journal Letters, 784, L28. http://stacks.iop.org/2041-8205/784/i=2/a=L28

Nakar, E. 2007, Phys. Rept., 442, 166

Narayan, R., Paczynski, B., & Piran, T. 1992, ApJL, 395, L83

Nicholl et al. 2017, The Astrophysical Journal Letters, 848, L18. http://stacks.iop.org/2041-8205/848/i=2/a=L18

Nordin, J., Brinnel, V., Van Santen, J., et al. 2019, Astronomy & Astrophysics, 631, A147

O'Connor, B., Troja, E., Dichiara, S., et al. 2020, arXiv preprint arXiv:2012.00026

Oke, J., Cohen, J., Carr, M., et al. 1995, Publications of the Astronomical Society of the Pacific, 107, 375

Pedregosa, F., Varoquaux, G., Gramfort, A., et al. 2011, Journal of Machine Learning Research, 12, 2825

Pérez, F., & Granger, B. E. 2007, Computing in Science and Engineering, 9, 21. https://ipython.org

Pian, E., D'Avanzo, P., Benetti, S., et al. 2017, Nature, 551, 67

Rastinejad, J. C., Fong, W., Kilpatrick, C. D., et al. 2021, ApJ, 916, 89

Rau et al. 2009, Publications of the Astronomical Society of the Pacific, 121, 1334. http://stacks.iop.org/1538-3873/121/i=886/a=1334

Reusch, S., Ahumada, T., Anand, S., et al. 2020a, GRB Coordinates Network, 27745, 1

Reusch, S., Andreoni, I., Kumar, H., et al. 2020b, GRB Coordinates Network, 28981, 1

Rhodes, L., Fender, R., Williams, D. R. A., & Mooley, K. 2021, MNRAS, 503, 2966

Rigault, M., Neill, J. D., Blagorodnova, N., et al. 2019, Astronomy Astrophysics, 627, A115. http://dx.doi.org/10.1051/0004-6361/201935344

Rossi, A., Rothberg, B., Palazzi, E., et al. 2021, arXiv e-prints, arXiv:2105.03829

Rosswog, S. 2015, Int. J. Mod. Phys., D24, 1530012

Ryan, G., Van Eerten, H., Piro, L., & Troja, E. 2020, The Astrophysical Journal, 896, 166

Shappee, B. J., Simon, J. D., Drout, M. R., et al. 2017, Science, 358, 1574

Singer et al. 2013, The Astrophysical Journal Letters, 776, L34. http://stacks.iop.org/2041-8205/776/i=2/a=L34

—. 2015, The Astrophysical Journal, 806, 52

Smartt, S. J., Chen, T.-W., Jerkstrand, A., et al. 2017, Nature, 551, 75

Smartt et al. 2017, Nature, 551, 75 EP . http://dx.doi.org/10.1038/nature24303

Steele, I. A., Smith, R. J., Rees, P. C., & Baker, I. P. 2004, The Liverpool Telescope: performance and first results, , , doi:10.1117/12.551456. https://doi.org/10.1117/12.551456

Stein, R., Reusch, S., & Necker, J. 2021, desy-multimessenger/nuztf: v2.4.1, vv2.4.1, Zenodo, doi:10.5281/zenodo.5758176. https://doi.org/10.5281/zenodo.5758176

Stein, R., Velzen, S. v., Kowalski, M., et al. 2021, Nature Astronomy, 5, 510

Stern, D., Assef, R. J., Benford, D. J., et al. 2012, The Astrophysical Journal, 753, 30. http://stacks.iop.org/0004-637X/753/i=1/a=30

Svinkin, D., Golenetskii, S., Aptekar, R., et al. 2020, GRB Coordinates Network, 27755, 1

Tachibana & Miller. 2018, Submitted to PASP

Tanvir, N. R., Levan, A. J., González-Fernández, C., et al. 2017, ApJL, 848, L27

Tonry, J. L. 2011, Publ. Astron. Soc. Pac., 123, 58

Troja, E., Piro, L., van Eerten, H., et al. 2017, Nature, 551, 71 EP . http://dx.doi.org/10.1038/nature24290

Troja, E., Piro, L., van Eerten, H., et al. 2017, Nature, 551, 71

Troja, E., Castro-Tirado, A. J., Becerra González, J., et al. 2019, Monthly Notices of the Royal Astronomical Society, 489, 2104

Tsutsui, R., Yonetoku, D., Nakamura, T., Takahashi, K., & Morihara, Y. 2013, Monthly Notices of the Royal Astronomical Society, 431, 1398

Van Rossum, G., & Drake, F. L. 2009, Python 3 Reference Manual (Scotts Valley, CA: CreateSpace)

Vieira, N., Ruan, J. J., Haggard, D., et al. 2020, arXiv e-prints, arXiv:2003.09437

Virtanen, P., Gommers, R., Oliphant, T. E., et al. 2020, Nature Methods, 17, 261

von Kienlin, A., Meegan, C. A., Paciesas, W. S., et al. 2020, ApJ, 893, 46

von Kienlin, A., Meegan, C., Paciesas, W., et al. 2020, The Astrophysical Journal, 893, 46

Wijers, R. A. M. J., Rees, M. J., & Mészáros, P. 1997, Monthly Notices of the Royal Astronomical Society, 288, L51. http://dx.doi.org/10.1093/mnras/288.4.L51

Willingale, R., O'Brien, P. T., Osborne, J. P., et al. 2007, The Astrophysical Journal, 662, 1093

Woosley, S. E., & Bloom, J. S. 2006, ARA&A, 44, 507

Wright, E. L., Eisenhardt, P. R. M., Mainzer, A. K., et al. 2010, The Astronomical Journal, 140, 1868. http://stacks.iop.org/1538-3881/140/i=6/a=1868

Yao, Y., Miller, A. A., Kulkarni, S., et al. 2019, The Astrophysical Journal, 886, 152

Zhang, & Choi. 2008, Astronomy and Astrophysics, 484, 293. https://doi.org/10.1051/0004-6361:20079210

Zhang, B. B., Liu, Z. K., Peng, Z. K., et al. 2021, Nature Astronomy, 5, 911

Zhang, Z., Chen, D., & Huang, Y. 2012, The Astrophysical Journal, 755, 55

Table 4. Follow-up table of the candidates identified for GRB 180523B, some of them reported in Coughlin et al. (2018b). The spectroscopic (s) or photometric (p) redshifts of the respective host galaxies are listed as well. The photometric slow evolution of some candidates was used as a rejection criteria when the object presents a variation on its magnitude smaller than 0.3 mag/day.

Name	RA	Dec	Discovery magnitude	Redshift	rejection criteria
ZTF18aawozzj	12:31:09.02	+57:35:01.8	g = 20.20	(s) 0.095	SN Ia-91T P200
ZTF18aawnbgg	10:40:54.05	+23:44:43.3	r = 19.80	(s) 0.135	SN Ia P200
ZTF18aawmvbj	10:12:41.17	+21:24:55.5	r = 19.75	(s) 0.14	SN Ia P200
ZTF18aawcwsx	10:40:33.46	+47:02:24.4	r = 19.84	(s) 0.09	SN Ia-91T P60
ZTF18aawnbkw	10:38:47.66	+26:18:51.8	r = 19.91	(p) 0.31	slow SDSS
ZTF18aawmqwo	09:52:06.90	+47:18:34.8	r = 19.98	(p) 0.04	slow SDSS
ZTF18aawmkik	08:51:11.45	+13:13:16.7	r = 19.04	(p) 0.52	slow SDSS
ZTF18aawnmlm	11:03:11.38	+42:07:29.9	r = 20.12	orphan	slow flat in 7 days
ZTF18aauhzav	10:59:29.32	+44:10:02.7	r = 19.97	(s) 0.05	slow 2MASX
ZTF18aavrhqs	11:58:09.57	+63:45:34.6	r = 19.99	orphan	slow
ZTF18aawmwwk	10:35:26.51	+65:22:34.3	r = 19.99	(p) 0.18	slow SDSS
ZTF18aawwbwm	08:16:44.98	+35:34:13.1	r = 19.79	(p) 0.15	slow SDSS
ZTF18aawmjru	08:39:11.39	+44:01:53.6	r = 18.43	(p) 0.44	slow SDSS
ZTF18aawmigr	08:48:01.76	+29:13:51.9	r = 19.63	(s) 0.1	slow 2MASX

Table 5. Follow-up table of the candidates identified for GRB 180626C, some reported in Coughlin et al. (2018a). The spectroscopic (s) or photometric (p) redshifts of the respective host galaxies are listed as well. The photometric slow evolution of some candidates was used as a rejection criteria when the object presents a variation on its magnitude smaller than 0.3 mag/day.

Name	RA	Dec	Discovery magnitude	Redshift	rejection criteria
ZTF18aauebur	19:48:49.10	+46:30:36.1	r = 18.85	stellar	CV multiple previous bursts

Table 6. Follow-up table of the candidates identified for GRB 180715B, some of them reported in Cenko et al. (2018). The spectroscopic (s) or photometric (p) redshifts of the respective host galaxies are listed as well. The photometric slow evolution of some candidates was used as a rejection criteria when the object presents a variation on its magnitude smaller than 0.3 mag/day.

Name	RA	Dec	Discovery magnitude	Redshift	rejection criteria
ZTF18aamwzlv	13:06:44.59	+68:59:52.9	r = 18.50	(s) 0.1	slow
ZTF18abhbevp	14:21:00.83	+72:11:43.8	g = 20.63	–	slow
ZTF18abhbpkm	16:02:36.78	+70:47:05.1	g = 21.24	–	slow
ZTF18abhhjyd	13:02:32.07	+75:16:49.4	g = 20.43	–	AGN Milliquas match
ZTF18abhbgan	15:43:18.86	+72:05:24.8	g = 21.22	orphan	slow
ZTF18abhbfoi	13:24:34.01	+70:56:47.5	g = 21.12	(s)1.2	AGN Milliquas and PS1
ZTF18abhbcjy	14:20:50.39	+73:25:40.5	g = 20.78	–	slow
ZTF18abhaogg	13:42:45.47	+74:19:38.3	r = 20.38	orphan	slow
ZTF18abhbamj	15:26:58.78	+72:02:17.8	r = 21.27	orphan	slow
ZTF18abhawjn	13:31:27.33	+66:46:45.4	g = 20.69	(s) 0.4	AGN Milliquas
ZTF18abharzk	13:41:09.05	+70:43:06.8	r = 21.30	–	slow
ZTF18abhbckn	12:49:53.85	+73:02:00.5	r = 20.93	(s) 0.00541	slow CLU
ZTF18abhbfqf	13:16:00.24	+69:37:24.1	r = 19.80	(s) 0.11	SN Ia-91T P200
ZTF18aauhpyb	13:21:45.49	+70:55:59.8	g = 19.67	stellar	CV multiple bursts P60

Table 7. Follow-up table of the candidates identified for GRB 180913A, some of them reported in Coughlin et al. (2018b). The spectroscopic (s) or photometric (p) redshifts of the respective host galaxies are listed as well. The photometric slow evolution of some candidates was used as a rejection criteria when the object presents a variation on its magnitude smaller than 0.3 mag/day.

Name	RA	Dec	Discovery magnitude	Redshift	rejection criteria
ZTF18abvzgms	23:37:50.57	+47:53:21.2	g = 21.29	(p) 0.35	flat evolution SDSS
ZTF18abwiios	23:12:14.06	+39:27:50.6	g = 22.04	–	flat evolution
ZTF18abvzfgy	23:16:15.20	+43:31:59.3	g = 20.98	(s) 0.04	SN Ic DCT
ZTF18abvzjwk	22:30:32.49	+39:50:14.6	g = 21.70	orphan	flat evolution
ZTF18abvwhkl	23:05:44.17	+45:32:34.8	r = 21.44	–	flat evolution 3 points
ZTF18abvucnv	22:31:31.96	+39:30:03.7	r = 21.15	stellar	Star flare
ZTF18abwiitm	23:15:27.61	+39:57:10.5	g = 21.71	–	slow AGN WISE
ZTF18abvubdm	22:58:28.45	+47:06:03.8	g = 21.01	–	slow evolution nice lc
ZTF18abvzsld	00:15:57.12	+49:28:51.0	g = 21.50	Stellar	flat evolution
ZTF18abwiivr	22:52:15.80	+37:22:29.4	g = 21.73	Stellar	slow evolution
ZTF18abvzmtm	23:55:13.07	+48:21:37.8	g = 21.65	orphan	slow

Table 8. Follow-up table of the candidates identified for GRB 181126B , reported in Ahumada et al. (2018). The spectroscopic (s) or photometric (p) redshifts of the respective host galaxies are listed as well. The photometric slow evolution of some candidates was used as a rejection criteria when the object presents a variation on its magnitude smaller than 0.3 mag/day.

Name	RA	Dec	Discovery magnitude	Redshift	rejection criteria
ZTF18achtkfy	06:54:02.63	+37:04:28.6	g = 19.69	orphan	slow
ZTF18achflqs	04:41:09.49	+23:53:24.9	r = 20.20	(p) 0.38	flat evolution SDSS
ZTF18acrkcxa	04:55:02.52	+22:40:43.4	r = 20.85	Stellar	Flare Keck LRIS
ZTF18acrkkpc	06:23:15.56	+10:19:22.6	r = 20.17	(s) 0.061	SN II Keck LRIS
ZTF18aadwfrc	06:17:18.02	+50:29:03.3	r = 19.65	(s) 0.04	SN Ia-02cx Keck LRIS
ZTF18acrfond	03:59:26.95	+24:35:20.4	r = 10.13	(s) 0.117	SN Ia Keck LRIS
ZTF18acrfymv	06:18:01.18	+44:10:52.7	g = 20.82	(s) 0.072	SN Ic-BL Keck LRIS
ZTF18acptgzz	04:33:32.45	-01:38:51.1	r = 19.56	(s) 0.096	SN Ia Keck LRIS
ZTF18acbyrll	05:55:28.67	+29:28:20.3	r = 19.34	orphan	slow evolution
ZTF18acrewzd	04:41:17.29	-01:46:07.5	g = 20.74	(s) 0.13	SN Ia Keck LRIS

Table 9. Follow-up table of the candidates identified for GRB 200514B , reported in Ahumada et al. (2020) and Reusch et al. (2020a). The spectroscopic (s) or photometric (p) redshifts of the respective host galaxies are listed as well. The photometric slow evolution of some candidates was used as a rejection criteria when the object presents a variation on its magnitude smaller than 0.3 mag/day.

Name	RA	Dec	Discovery magnitude	Redshift	rejection criteria
ZTF20aazpphd	242.7149675	+27.1616870	r = 19.6		slow
ZTF20aazppnv	238.1438691	+25.5764946	r = 21.1	(p) 0.17	slow
ZTF20aazprjq	233.5213585	+43.3298714	r = 21.3	(p) 0.23	slow
ZTF20aazptlp	229.007524	+48.774925	r = 21.5	(p) 0.40	slow
ZTF20aazptnn	237.2967278	+47.271954	r = 21.6	(p) 0.26	slow
ZTF20aazpnst	254.0989833	+34.4655542	r = 22.0	(p) 0.19	slow
ZTF20aazpofi	236.929525	+46.9809542	r = 21.5	(p) 0.46	slow
ZTF20aazplwp	2734.0167814	41.1672761	r = 21.6		slow
ZTF20aazqlgx	2746.0908608	34.6259478	r = 22.3	(p) 0.35	slow
ZTF20aazphye	2755.6577428	41.7013160	r = 21.6	(p) 0.26	slow
ZTF20aazpnxd	2755.931646	48.3862806	r = 21.6		slow
ZTF20aazpkri	2740.7324792	48.5554957	r = 21.3		slow
ZTF20aazqndp	2737.8212032	50.4933039	r = 22.1	(s) 0.03	slow
ZTF20aazqpps	2752.2388065	41.3097433	r = 21.6	(s) 0.2	slow

Table 10. Follow-up table with the candidate identified for GRB 210510A, reported in Anand et al. (2021). The spectroscopic (s) of the respective host galaxy are listed as well.

Name	RA	Dec	Discovery magnitude	Redshift	rejection criteria
ZTF21abaytuk	13:48:49.89	+35:32:13.05	g = 21.76	(s) 0.8970	AGN Keck LRIS

Table 11. Follow-up table of the candidates identified for GRB 210529B , reported in Ahumada et al. (2021). The spectroscopic (s) or photometric (p) redshifts of the respective host galaxies are listed as well. The photometric slow evolution of some candidates was used as a rejection criteria when the object presents a variation on its magnitude smaller than 0.3 mag/day.

Name	RA	Dec	Discovery magnitude	Redshift	rejection criteria
ZTF21abcwmzx	14:42:28.10	+31:56:34.19	g = 21.51	–	slow
ZTF21abcwnbm	14:43:43.24	+33:44:52.20	g = 21.54	–	slow
ZTF21abcwuxv	15:30:34.50	+43:05:52.27	r = 21.82	orphan	slow
ZTF21abcwvzr	14:49:49.23	+35:05:43.32	r = 21.9	–	slow
ZTF21abcwwaj	14:40:59.49	+32:07:24.64	r = 21.24	(s)0.1	slow
ZTF21abcwyoe	15:58:56.54	+33:08:01.79	r = 21.83	–	slow
ZTF21abcwyvi	15:58:53.27	+33:39:12.74	r = 21.98	–	slow